CHALMERS
UNIVERSITY OF TECHNOLOGY

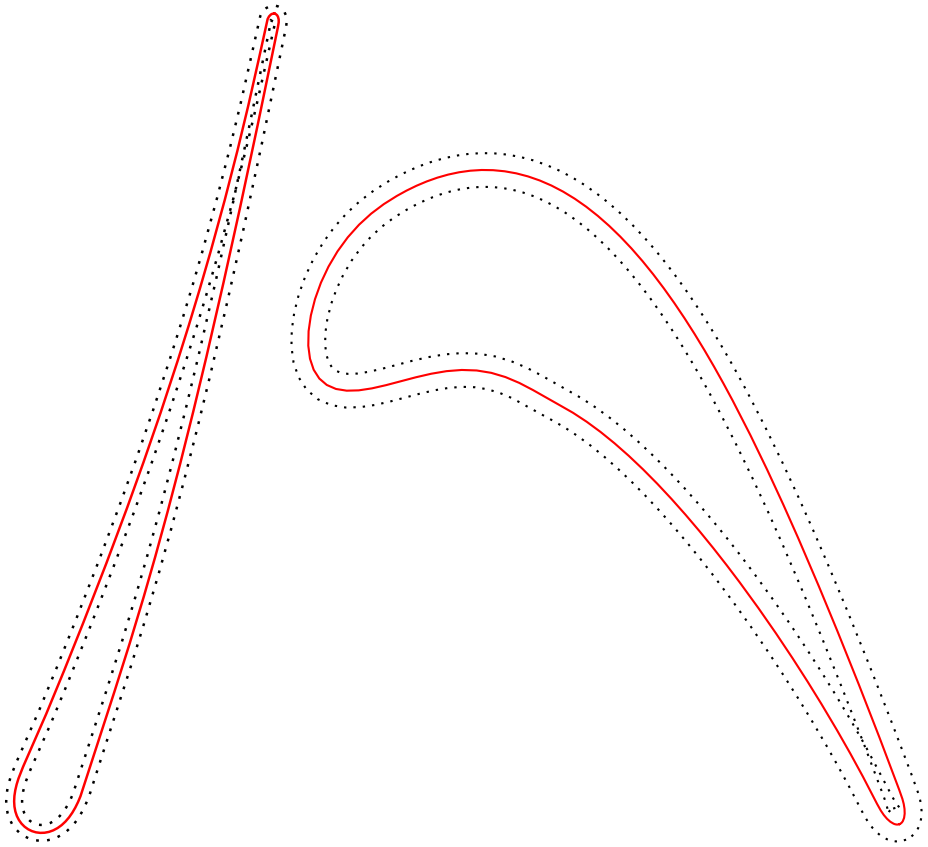

A Study on the Impact of Blade Tolerances on Turbine Performance

Master's Thesis in Sustainable Energy Systems

PATRICK NILSSON

Department of Applied Mechanics
CHALMERS UNIVERSITY OF TECHNOLOGY
Gothenburg, Sweden 2016

Master's Thesis in Sustainable Energy Systems

A Study on the Impact of Blade Tolerances on Turbine Performance

PATRICK NILSSON

CHALMERS
UNIVERSITY OF TECHNOLOGY

Department of Applied Mechanics
Division of Fluid Dynamics
Chalmers University of Technology
Gothenburg, Sweden 2016

A Study on the Impact of Blade Tolerances on Turbine Performance
Patrick Nilsson

Supervisors: Pieter Groth and Martin Olausson, GKN Aerospace
Examiner: Niklas Andersson, Department of Applied Mechanics

Master's Thesis 2016:81
ISSN 1652-8557
Department of Applied Mechanics
Division of Fluid Dynamics
Chalmers University of Technology
SE-412 96 Gothenburg
Sweden
Telephone: +46 (0)31-772 1000

Cover: Blade profiles and manufacturing tolerances for stator (left) and rotor (right) turbine blades. The solid (red) line represents nominal blade profile, while the dotted (black) line represents manufacturing tolerances.

Typeset in LaTeX
Department of Applied Mechanics
Gothenburg, Sweden 2016

The Impact of Blade Tolerances on Turbine Performance
Master's Thesis in Sustainable Energy Systems
Patrick Nilsson
Department of Applied Mechanics
Division of Fluid Dynamics
Chalmers University of Technology

Abstract

When manufacturing blades, there is a need for tolerancing around nominal blade design. Tolerance design is a balance between turbine performance and cost efficiency; a tolerance band that is too wide will result in a large scatter in turbine characteristics, whereas a too narrow tolerance band leads to high manufacturing costs due to high scrap rates of blades not meeting requirements. Determining an optimal manufacturing tolerance is therefore an issue of great importance. The purpose of this thesis was to study the impact of geometric variability within manufacturing tolerances on turbine performance.

This Master's Thesis was conducted at the Department of Rotors at GKN Aerospace in Trollhättan, Sweden. In this thesis, a rational method has been developed to vary blade profiles of both stator and rotor blades within current manufacturing tolerances at GKN Aerospace. Blade profiles are modified using a sinusoidal profile variation, which allows variation of amplitude A_i, period n_i, and phase angle φ_i, to model manufacturing variations within profile tolerance limits. The method has been utilised to study the impact of simulated manufacturing tolerances on turbine performance through CFD simulations. Several design cases were produced by variations of the function used to produce sinusoidal profile variations, and evaluated in the project. It was seen that limiting curves for flow function Q were characterised by stator-rotor configurations for minimum-minimum and maximum-maximum profile tolerance, while limiting curves for efficiency η where characterised by stator-rotor configurations for minimum-maximum and maximum-minimum profile tolerances. The impact of subsequent design cases for profile variations within manufacturing tolerances fell within these limiting curves. Certain blade design parameters, such as trailing edge thickness and unguided trailing edge, were identified as key parameters with respect to impact on turbine performance.

Keywords: tolerancing, tolerance optimisation, robust design, blade design, turbine performance, optimisation, profile variation, geometric variability, manufacturing tolerances

Acknowledgements

I would like to express my gratitude to my supervisors at GKN Aerospace, Pieter Groth and Martin Olausson, for the opportunity of doing my thesis with them at GKN Aerospace, as well as for their continuous support and guidance during this time. A special thanks to the Department of Rotors for making me feel welcome.

I would also like to thank my examiner, Niklas Andersson; for his input and for stepping in to examine this thesis on such short notice.

Thank you to all of the friends I have made during my years at Chalmers University of Technology for making these years so memorable; no names, no pack drill.

Finally, I reserve my deepest gratitude to my family and to my partner, Malin, for their unwavering and unyielding support throughout my years of study. This accomplishment would not have been made possible without them. Thank you for always believing in me.

Patrick Nilsson, Gothenburg, November 2016

Nomenclature

Abbreviations

CFD	Computational fluid dynamics
DOE	Design of Experiments
LE	Leading edge
LHS	Latin hypercube sampling
RANS	Reynolds-averaged Navier–Stokes
RSM	Response surface methodology
TE	Trailing edge
TED	Turbine exhaust duct

Greek symbols

Variable	Description	Unit
γ	Heat capacity ratio	–
μ	Dynamic viscosity	$\frac{Ns}{m^2}$
η	Efficiency	–
Π	Total pressure ratio	–
ρ	Density	kg/m^3
Φ	Viscous dissipation function	–
φ	Phase angle	$^\circ$
θ	Tangential direction	–
$r\theta$	Polar angle (polar coordinate)	–

Roman symbols

Variable	Description	Unit
A	Stage area	m^2
$A_{channel}$	Channel area	m^2
A_i	Amplitude	
C_e	Trailing edge coefficient	–
C_p	Specific heat capacity	J/K
f	Body forces	m/s^2
H	Channel height	m
h	Enthalpy	J/kg
h_0	Stagnation enthalpy	J/kg
m	Number of variables to be sampled	–
$\dot{m}$	Mass flow rate	kg/s
N	Rotational speed	rpm
n	Period	–
P	Pressure	Pa
p	Number of samples	–
Q	Flow function	–
R	Gas constant	$J/(kgK)$
r	Radial distance (polar coordinate)	m
r_m	Mean gas radius	m
s	Entropy	$J/(kgK)$
s_i	Length along blade profile	m
s_N	Blade profile circumference	m
T	Temperature	K

$\widehat{\mathbf{T}}$	Tangent vector	–
t	Time	s
U	Instantaneous velocity	m/s
u	Fluctuating velocity	m/s
x	Cartesian coordinate	–
y	Cartesian coordinate	–
z	Cartesian coordinate	–
$\langle U \rangle$	Mean velocity	m/s
$\langle u_i u_j \rangle$	Reynolds stress	m^2/s^2

Dimensionless numbers

Variable	Description	Definition
Pr	Prandtl number	$Pr = \frac{C_p \mu}{\lambda}$
Re	Reynolds number	$Re = \frac{\rho L U}{\mu}$

Subscripts

in	Inlet
max	Maximum
min	Minimum
out	Outlet
0	Stagnation properties
i	Stator or rotor
r	Rotor
s	Stator

Superscripts

$'$	Isentropic properties

Software

2LOOP	Method to investigate blade tolerance impact on turbine performance
G3dMesh	Structured multi-block grid generator
VolSol++	Block-structured, compressible Navier-Stokes solver
modeFRONTIER	Multiobjective optimisation tool, commercial software
theLOOP	Blade optimisation method for compressor and turbine blades
Python	High-level general-purpose programming language
PollyGraph	Blade design tool used for geometry generation

Contents

List of Figures

List of Tables

1

Introduction

In preliminary engine design for aircraft and spacecraft propulsion, a number of steps are required before reaching an optimal design. In spacecraft propulsion, typical design challenges include handling extreme loads, temperatures, and transients within the engine while maintaining a high power-to-weight ratio. Furthermore, engines need to be highly reliable and cost efficient due to an increasingly competitive market.

GKN Aerospace has since the 1970's taken part in producing many of the rocket engines used by the European Space Agency (ESA), including over 250 turbines to date for the Ariane project. In 2016, GKN Aerospace secured contracts with Airbus Safran Launchers to develop and manufacture rocket engine sub-systems for the Ariane 6 launcher [1].

Currently, a new expander cycle engine known as the Vinci rocket engine is being developed for use as an upper stage engine. In the process of rocket propulsion, it uses liquid oxygen (LOx) and liquid hydrogen (LH_2) as propellants. GKN Aerospace is responsible for developing the LH_2 and LOx turbines. Challenges associated with this development is the focus of this thesis.

During manufacturing of turbine blades for spacecraft propulsion engines at GKN Aerospace, a certain variability of blade dimensions is inevitable. In order to ensure production cost efficiency *and* performance of the turbine, one option is setting a tolerance band around nominal blade dimensions. However, a too wide band will result in a large scatter in turbine characteristics (such as torque, efficiency, pressure drop, etc.), whereas a too narrow tolerance band leads to high manufacturing costs due to high scrap rates of blades not meeting requirements. Determining an optimal manufacturing tolerance is therefore an issue of great importance.

1.1 Aim

The purpose of this thesis was to develop a rational method for studying the impact of manufacturing tolerances on turbine performance. This included the formulation of a method for simulating blades with geometric variability. The impact of geometry variations within manufacturing tolerances for turbine blade profiles, i.e. the shape of the blades, was studied to show the applicability and potential of the method.

The purpose of the project may be clarified through the following objectives:

- To develop a rational method to vary blade profile
- To study the impact of geometry variations on performance of turbine blades
- To demonstrate the applicability of the method as a potential tool for decision making on manufacturing tolerances

1.2 Constraints

The project concerns a single-staged expander cycle liquid hydrogen (LH_2) turbine. Downstream of the turbine stage, the fluid exits the turbine through the turbine exhaust duct (TED) via a sharp bend. This sharp bend causes rapid expansion of the fluid and a highly turbulent flow that is complex and difficult to simulate. The geometry of the turbine was therefore simplified as a straight duct as the focus of the thesis is on the effects on performance over the turbine stage, and not downstream of the stage.

Furthermore, the clearance gap between the rotor blades and turbine casing was discarded in all of the simulations in order to simplify the model. Furthermore, simulating generated blades which deviate from nominal design, the assumption was made that all of the blades within a row have the same geometric variation. By making this assumption it is sufficient to model one blade passage only for each blade row and employ periodic conditions to simulate the whole stage.

2

Theory

This chapter aims to provide the reader with an introduction to the background and theory of the project necessary in order to understand the setting. The reader is first introduced to basic principles of turbomachinery and liquid rocket engine turbines, which are the focus of the project. Following this, an overview of the current blade optimisation tool in use at GKN Aerospace (theLOOP) is presented with the theory of Latin hypercube sampling. The basic concepts of fluid dynamics are then summarised, and finally, a review of turbine design and performance analysis is given.

2.1 Basic principles of turbomachinery

Dixon and Hall [2] define a turbomachine as a machine which either transfers energy to or from a fluid through rotating blade rows. Examples of common turbomachines include for example compressors and turbines. In a typical gas turbine cycle, the fluid undergoes a series of thermodynamic processes, including compression, heat addition, and expansion; this is typically achieved through a compressor, a combustion chamber, and a turbine, respectively. The most basic gas turbine cycle is the Brayton cycle, which is shown in Figure 2.1 along with its principal components.

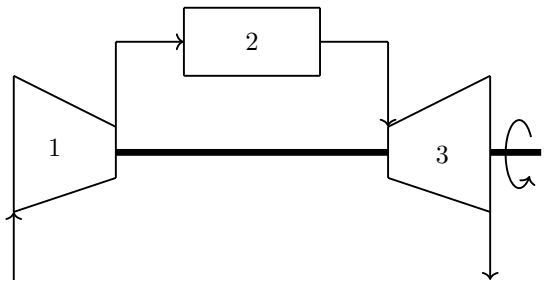

Figure 2.1: Simple Brayton gas turbine cycle consisting of (1) compressor, (2) combustion chamber, and (3) turbine.

Many times, when referring to "gas turbines" or simply "turbines", one is referring to an entire cycle, such as that in Figure 2.1. However, it should be clarified that in the scope of this project, it is only the turbine (3) that is considered.

2.1.1 Turbine components

As mentioned in Section 2.1, a turbomachine may transfer energy to *or* from a fluid. The direction of energy transfer is dependent on the machine being considered. As also mentioned, the turbomachine at focus in this project is a turbine; a turbine is used to transfer energy *from* the fluid. A turbine consists of one or more rows of blades, which may be stationary or rotary. Stationary blades are referred to as *stators* and serve to guide the fluid. Rotating blades are referred to as *rotors*. When a fluid passes a rotor row, it causes the blades to move. The rotational energy produced by the rotor rows is transferred to a shaft, resulting in power production. Simultaneously, the fluid is expanded to a lower pressure.

Rows of stator blades and rotor blades are alternated, and a stator row and a rotor row together make up a *stage*. A turbine may be either single-staged or multiple-staged depending on the requirements and demands set for the turbine.

2.1.2 Liquid rocket engine turbines

The turbine considered within this project is one designed for spacecraft propulsion. Herein follows a brief overview of liquid rocket engine turbines that exist today. There are three main types of turbopump driven engines for spacecraft propulsion; staged combustion cycles, gas generator cycles, and expander cycles, as shown in Figure 2.2. In staged combustion cycles (2.2a), the fuel is pumped through a nozzle, where heat exchange serves to preheat the fluid. The following passage through a preburner partially combusts the fuel in a rich mixture. The exhaust gases are then sent to a turbine, where their expansion is used to power oxidiser and fuel pumps, before finally arriving at the combustion chamber responsible for spacecraft propulsion. Gas generator cycles (2.2b), on the other hand, utilise gas generators instead of preburners for combustion-free production of the hot gas that is used to drive the turbine. In this case, separate fractions of the fuel are used to drive the turbine and propel the rocket. As not all of the propellant is sent to the combustion chamber, the gas generator cycle is referred to as an open cycle (as opposed to staged combustion cycles or expander cycles, which are so called closed cycles). Lastly, in expander cycles (2.2c), the preheated fuel is used to drive the turbine directly, without the need for a preburner or gas generator. The fuel is then injected into the combustion chamber and used for propulsion.

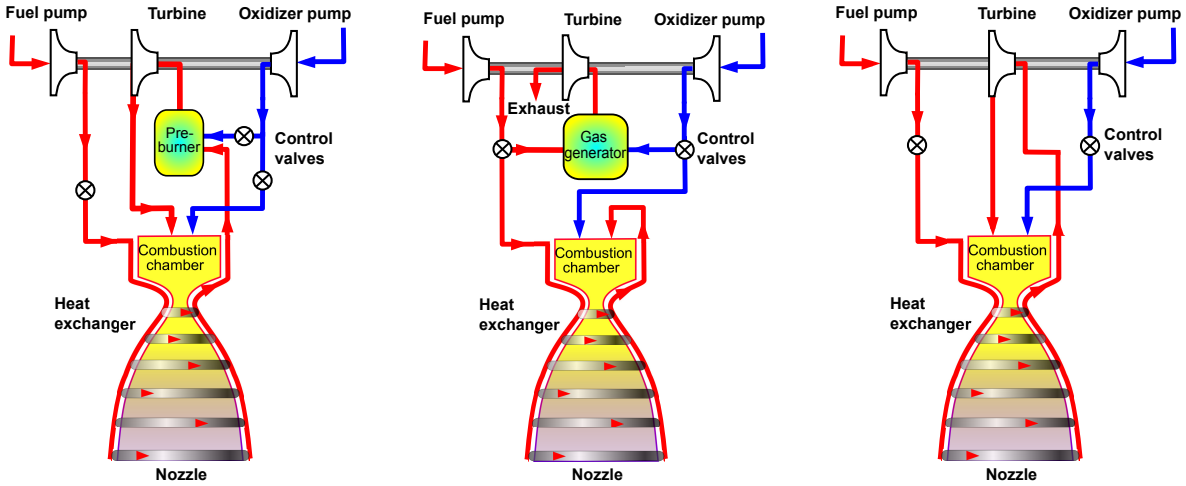

(a) Staged Combustion Cycle [3] **(b)** Gas Generator Cycle [4] **(c)** Expander cycle [5]

Figure 2.2: Rocket thermodynamic cycles for spacecraft propulsion

2.2 theLOOP

When designing compressor and turbine blades, GKN Aerospace uses an in-house blade optimisation method known as theLOOP. The method developed within this project is designed in a similar manner as done in theLOOP, and a brief background to the method is therefore provided in the following section.

theLOOP is not a fully automated optimisation loop, but a set of Python programs that generate geometries, create meshes, run CFD simulations, and post-process results to be used in modeFRONTIER. Figure 2.3 shows an infographic of the blade optimisation method theLOOP to visualise the different components in the method.

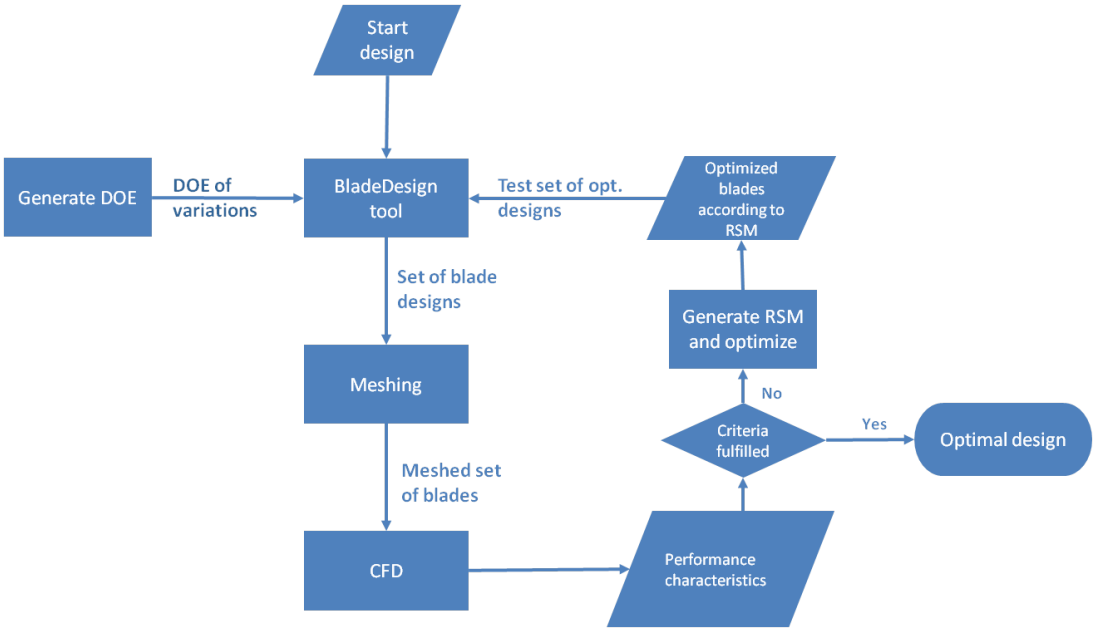

Figure 2.3: Infographic of theLOOP, a blade optimisation method developed and used by GKN Aerospace when designing compressor and turbine blades. Courtesy of GKN Aerospace [6].

The initial phase of theLOOP involves generating a design of experiments (DOE) table, which is done with the help of modeFRONTIER, a multiobjective optimisation software. Prior to creating the DOE table, one chose which blade parameters to vary and their range of variation. Permissible blade parameters depend on the parametrization used for the blade. Variations of each blade parameter are generated through Latin hypercube sampling (see Section 2.2.1). After the design table has been generated, the main program of theLOOP, which reads the DOE table and sends jobs to subprograms, is executed. The subprograms read the DOE table, create the blade geometries and meshes, run CFD simulations using in-house solvers, and post-process the results once simulations are done. The post-processed results are retrieved by the main program, which writes the results to a design table, containing the information in the DOE table as well as the resulting performance characteristics and other objectives for each considered blade configuration.

The design table may be used to to generate a response surface in e.g. modeFRONTIER. Response surface methodology (RSM) involves examining and evaluating relationships between the design variables and response variables. The response variables are defined by the user and dependent on what parameter that is to be optimised. The purpose of RSM is to use the DOE to find and optimal response, or in this case, an optimal blade design. The RSM may therefore be used to generate a new design table to be run through theLOOP. If a designed blade meets all of the performance criteria, theLOOP is discontinued and an optimal blade design is obtained. [6]

2.2.1 Latin hypercube sampling

In the area of statistics and statistical sampling, there are various methods for sampling. Random sampling involves sampling with no conditions and samples are generated regardless of previous samples. On the other hand, Latin hypercube sampling, first described by McCay et al. [7], is a *near*-random statistical sampling method.

To understand this method, one could begin by considering an n-by-n array of values, which may be referred to as a *Latin square* if it fulfils certain conditions. The conditions for a Latin square is that each value in the array, or sample, may only be sampled exactly once in each row,

and exactly once in each column. To visualise this, one could for example consider the concept of *sudoku*, which samples the integers 1 through 9. Essentially, two conditions exist in order to solve a sudoku problem, where the first, and perhaps most simple, is that each integer in the range $n = 1, \ldots, 9$ may only occur once in each row, and once in each column (the second is that each integer may not be sampled more than once in each 3-by-3 subregion). The Latin *hypercube* follows the same principles as a Latin square, but is extended to an arbitrary number of dimensions.

As opposed to random sampling, which allows sampling irrespective of previous samples, Latin square and Latin hypercube sampling is dependent on previous samples. Also, the position of each sample in the square or cube has to be kept in mind, so as to avoid a sample reoccurring in a row or column more than once. Furthermore, Latin hypercube sampling requires that the number of variables (dimensions) m and the number of samples s required for each variable be defined prior to sampling, in order to divide the range of variables equally.

2.3 Fluid dynamics

Fluid dynamics is the study of fluids in motion. In this section, the governing laws of fluid dynamics, will be presented, followed by subsections dedicated to turbulent flow and a brief definition of computational fluid dynamics (CFD).

2.3.1 The Conservation Equations

The foundation of fluid dynamics is based on the law of conservation. To accurately describe and solve fluid dynamics problems, three conservation laws are defined, namely the conservation of mass, momentum, and energy, respectively. These conservation laws may be written in equation form, which are presented in Sections 2.3.1.1-2.3.1.3.

2.3.1.1 Conservation of Mass

Conservation of mass, based on the continuity equation, describes the notion that the accumulation of fluid mass within a given control volume must equal the rate of change of fluid mass across the control volume's boundaries; in layman's terms, mass cannot be created or destroyed. This continuity equation is given in tensor notation by [8]

$$\frac{\partial \rho}{\partial t} + \nabla \cdot (\rho U_i) = 0$$

2.3.1.2 Conservation of Momentum

Conservation of momentum discusses the rate of accumulation of momentum of a given control volume must equal the sum of the rate of change of momentum across the control volume's boundaries in addition to the sum of the external forces acting on the system. This is based on Newton's second law of motion, which states that the sum of the forces acting on an object is equal to the mass times the acceleration ($\sum F = ma$). The change in momentum in each respective direction must therefore be balanced by the net forces acting in the same direction. Balancing the momentum of the velocity component in each direction for a fluid element results in the Navier-Stokes equations, given in tensor notation as

$$\frac{\partial U_i}{\partial t} = f_i - \frac{\nabla P}{\rho}$$

where f_i represents surface and body forces.

2.3.1.3 Conservation of Energy

Similar to the conservation of mass, the law of conservation of energy states that energy cannot be created or destroyed; however, energy may be converted from one form to another. The balancing equation for total energy accounts for the rate of transport of energy to and from a system, as well as the work done on the system by the surroundings, and is given by [8]

$$\rho\frac{\partial h}{\partial t} = \frac{\partial P}{\partial t} + \nabla\cdot(k\nabla T) + \Phi$$

where h is the enthalpy, k is the thermal conductivity, and Φ is the function for viscous dissipation, which determines the rate of conversion of mechanical energy to heat.

2.3.2 Turbulent Flow

Depending on the nature of a flow, it may be characterised as laminar or turbulent. The Reynolds number, defined as the ratio of inertial force to viscous force, is typically used as a means of determining the flow characteristic. At high Reynolds numbers, the inertial forces exceed the viscous forces, causing irregular and random variations in the flow, and the flow is said be be turbulent.

Turbulent flows are distinguished by fluctuating velocity fields of small-scale, high-frequency fluctuations. In computational fluid dynamics, fully describing turbulent flows is computationally expensive, requiring large amounts of data and effort. Instead, the governing equations described in sections 2.3.1.1-2.3.1.3 may be rewritten to remove these fluctuations. In one such manipulation, instantaneous variables are separated into a mean and a fluctuating component, a concept called Reynolds decomposition. Velocity and pressure are decomposed accordingly as

$$U_i = \langle U_i\rangle + u_i \quad \text{and} \quad P = \langle P\rangle + p$$

where the instantaneous variable is the sum of the mean component and the fluctuating component. By ensemble-averaging the Reynolds decomposed Navier-Stokes equations, the Reynolds-averaged Navier-Stokes (RANS) equations are obtained. However, the introduction of the RANS equations gives rise to a closure problem due to the introduction of the unknown Reynolds stresses ($\rho\langle u_i u_j\rangle$), which are defined as a product of the velocity fluctuations introduced by the Reynolds decomposition of the instantaneous velocity. In order to close the set of equations, turbulence modelling can be used as a means of describing the Reynolds stresses. There are several methods for stress modelling that include transport equations for the turbulence quantities. These methods are generally classified according to the number of additional equations needed in excess of the RANS and continuity equations, i.e. zero-, one-, or two-equation models.

2.3.3 Computational Fluid Dynamics

Computational fluid dynamics involves numerical analysis of fluid flow; the conservation equations are solved numerically in conjunction with turbulence modelling. However, even though CFD simulations has been an important tool in this project, its fundamental theory will not be reviewed at any great length. Instead, the reader is assumed to have a basic understanding of the theory, or may otherwise refer to literature for this, such as Andersson et al [8].

2.4 Turbine Design

During the development process of a turbine, certain characteristics need to be evaluated in order to assess its performance, such as efficiency and mass flow which are covered herein. As the development progresses and more data is obtained, more reliable turbine characteristics may be computed to account for possible losses in performance, such as the energy output or power produced by the turbine. Blade design is an important element in turbine design and will be briefly covered as well.

2.4.1 Turbine performance analysis

At GKN Aerospace, dependent, or output, variables commonly considered when analysing turbine performance include mass flow, axial thrust, torque, and efficiency [9]. The input, or independent, variables are total-to-total pressure ratio across the turbine and rotor speed when the working fluid considered is an ideal gas. If the working fluid is a real gas, on the other hand, two additional input variables are considered, namely inlet total temperature and inlet total pressure. When studying the impact of blade tolerances on turbine performance, this will focus on the turbine efficiency, and the flow function, a dimensionless mass flow. These are presented in equation-form and described below. Furthermore, the turbine working fluid will be assumed to be an ideal gas, and the fluid thermodynamic properties are presented below as well.

2.4.1.1 Efficiency

Figure 2.4 shows an enthalpy-entropy diagram of a basic turbine expansion process. Entropy is a useful property within turbomachinery when characterising efficiency of a turbine or expansion process, as an increase in entropy corresponds to "lost work". In Figure 2.4, the line between 1–2 represents an actual expansion process while the line 1–2′ is the corresponding ideal or reversible process. As seen in the figure, the ideal or reversible process does not result in any increase in entropy, as opposed to the actual expansion process. In Figure 2.4, this is measurable by the distance between the initial point and the isentropic expansion point being greater than the distance between the initial point and the actual expansion point.

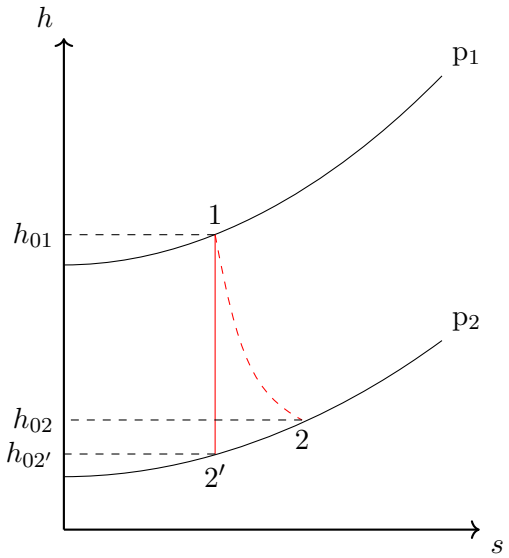

Figure 2.4: Enthalpy (h) versus entropy (s) diagram of a basic turbine expansion process. Point 1 denotes the turbine inlet while point 2 denotes the turbine outlet. $1-2'$ is referred to as an ideal or reversible process, in which entropy is constant, while $1-2$ is an actual expansion process in which entropy increases.

When characterising turbine efficiency many different definitions exist. In this project, efficiency is characterised in terms of the isentropic efficiency, which may be defined as the ratio of the amount (actual) work done upon the fluid to the ideal or maximum amount of work that could theoretically be achieved. The previous may be summarised in equation form in terms of the enthalpy drop across the turbine according to [2]

$$\eta = \frac{h_{01} - h_{02}}{h_{01} - h_{02'}} \tag{2.1}$$

where h_{01} and h_{02} are the stagnation enthalpies before and after the expansion process, and $h_{02'}$ is the isentropic enthalpy after the expansion.

For an ideal gas, the change in the enthalpy dh may be computed as

$$dh = \dot{m} C_p dT \tag{2.2}$$

where C_p is the gas' specific heat capacity, and dT is the change in temperature. Inserting this relation into equation (2.1) and assuming constant specific heat capacity and mass flow across the turbine expansion process yields

$$\eta = \frac{\Delta h_0}{\Delta h_{0'}} = \frac{\dot{m} C_p \Delta T_0}{\dot{m} C_p \Delta T_{0'}} = \frac{T_{01} - T_{02}}{T_{01} - T_{02'}} \tag{2.3}$$

In this report, when referring to efficiency η, it will be this definition of the isentropic total-to-total efficiency, that is referred to. No other efficiencies will be considered, and no other losses will be considered when calculating the efficiency.

Clearance gap losses

As mentioned briefly in Section 1.2, all turbomachines have a certain clearance gap between the turbine casing, and the rotating blades. This clearance gap results in tip leakage, which ultimately results in a reduction in work as the mass flow decreases. With a reduction in work, it becomes apparent that a decrease in efficiency is inevitable. By some estimates, with an increase in clearance gap by 1% of the blade height, the turbine suffers a $2 - 3\%$ loss in efficiency [2]. As also mentioned in Section 1.2, the clearance gap has been omitted in the model used in this project. Thus, it is important to keep in mind when analysing simulation results and efficiency values that any clearance gap losses are not accounted for, and that these values are not entirely accurate and representative of reality.

2.4.1.2 Flow function

When comparing simulations and results for different operating conditions, it is of interest to relate these using dimensionless variables because of the variations in turbine performance from one design to another. One such variable that will be considered in dimensionless form is the mass flow, $\dot{m}$. The dimensionless mass flow, referred to as the flow function Q is defined as

$$Q = \dot{m} \cdot \frac{\sqrt{R \cdot T_0}}{P_0 \cdot A_{channel}} \tag{2.4}$$

where $\dot{m}$ is the mass flow through the turbine, R is the gas constant, T_0 and P_0 are the total or stagnation temperature and pressure, respectively, at the turbine inlet, and $A_{channel}$ is the channel area. The channel area is calculated as

$$A_{channel} = 2\pi r_m H \tag{2.5}$$

where r_m is the mean gas radius and H is height of the flow channel.

If simulations and experiments can be accurately quantified in terms of dimensionless values, such as the flow function, the flow may be assumed to behave in a similar fashion in the real case. This gives the simulations results validity to accurately be used as basis for future decisions and designs.

2.4.2 Working-fluid properties

In this project, as the temperature and pressure drop across the single-stage turbine is limited, the working fluid is treated as a perfect gas in order to simplify simulations and calculations. Best practice guidelines when calculating expansion or compression processes in turbomachines suggest that weighted mean values for fluid properties corresponding to the mean temperaure of the process be used [2]. Table 2.1 lists constant fluid properties used for the simulations and calculations.

Table 2.1: Fluid thermodynamic properties for hydrogen used during the simulations. The working fluid was approximated as a perfect gas as the temperature and pressure drop across the turbine was limited.

Gas constant (R) $\left[\frac{J}{kgK}\right]$	4124
Heat capacity ratio (γ)	1.396
Dynamic viscosity (μ) $\left[\frac{Ns}{m^2}\right]$	$9 \cdot 10^{-6}$
Prandtl	0.72

2.4.3 Total pressure ratio

The total pressure ratio is simply defined as the ratio of the total or stagnation pressure between the turbine inlet and outlet, according to

$$\Pi = \frac{P_{0,in}}{P_{0,out}} \tag{2.6}$$

Henceforth, when referring to the pressure ratio Π, it will be this definition that is referred to, unless stated otherwise.

2.4.4 Blade profile design

When considering blade profile design, there are a number of design parameters that may be considered. While this project does not deal with blade design and generation of blades, there is value in introducing certain design criteria and best practice guidelines regarding these, in order to provide better understanding of the results

2.4.4.1 Leading and trailing edges

The blade trailing edge is responsible for controlling the exit flow conditions. The geometry of the trailing edge also helps determine the *throat*. The throat refers to the narrowest passage between two adjacent blades, as shown in Figure 2.5. If improperly sized, this can result in high exit losses, reducing the turbine performance [10]. To obtain a minimum amount of exit losses, it is recommended that the blade trailing edge radii, or thickness, be set to the smallest allowable, which is determined by stress limitations. [10]

The leading edge geometry is more critical in turbines where supersonic conditions are prevalent at the inlet. The inlet conditions for the turbine within the scope of this project are subsonic, and therefore the leading edge design is not as important as trailing edge design.

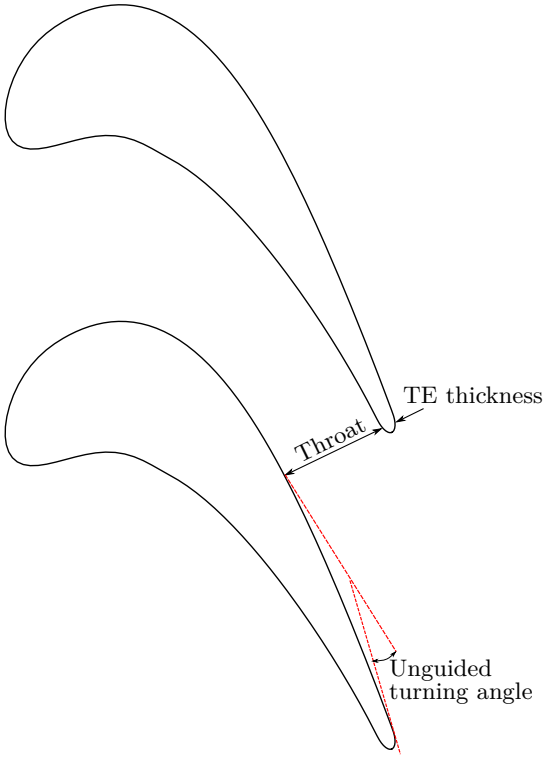

Figure 2.5: Diagram indicating the location of the throat and unguided turning angle. Unguided turning angle is defined as the difference in angle between the dashed (red) lines, which represent the two suction side tangents.

2.4.4.2 Unguided turning

Unguided turning, often employed in subsonic turbines, describes the phenomena in which the turning of the fluid, produced by the blade's suction side, continues after the fluid has passed the throat. This can be described by the difference in angle between two suction side tangents; one located at the throat, and one at the trailing edge, as visualised in Figure 2.5. This also results in a longer flow path which limits local accelerations along the profile, providing a smoother transition of fluid from leading to trailing edge. [10]

Recommended values of unguided turning are in the range $8 - 12^\circ$ at the blade hub (nearest the shaft) and up to 15° at the blade tip [10].

3

Method

The following chapter aims at giving an overview of the method used in the project. This includes a section dedicated to a brief overview of the method developed for studying the impact of blade tolerances on turbine performance (2LOOP), followed by more in-depth descriptions of its components and the tools used. Design cases in which the developed method is implemented and evaluated are presented as well as the CFD simulations and post-processing.

3.1 2LOOP

Similar to theLOOP (see Section 2.2), 2LOOP consists of a set of Python programs, in which main script reads the blade geometry file and the geometry variation design table and sends jobs to subscripts. As in theLOOP, subscripts read the design table, create the blade geometries with corresponding geometry variations, generate meshes, run CFD simulations using in-house solvers, and post-process the results once simulations are done. The results are written to file, and plots are generated for the geometry profiles as well as the performance variables presented in Section 2.4.1). Figure 3.1 shows a flow chart of how the the 2LOOP code is structured and general components involved in the method.

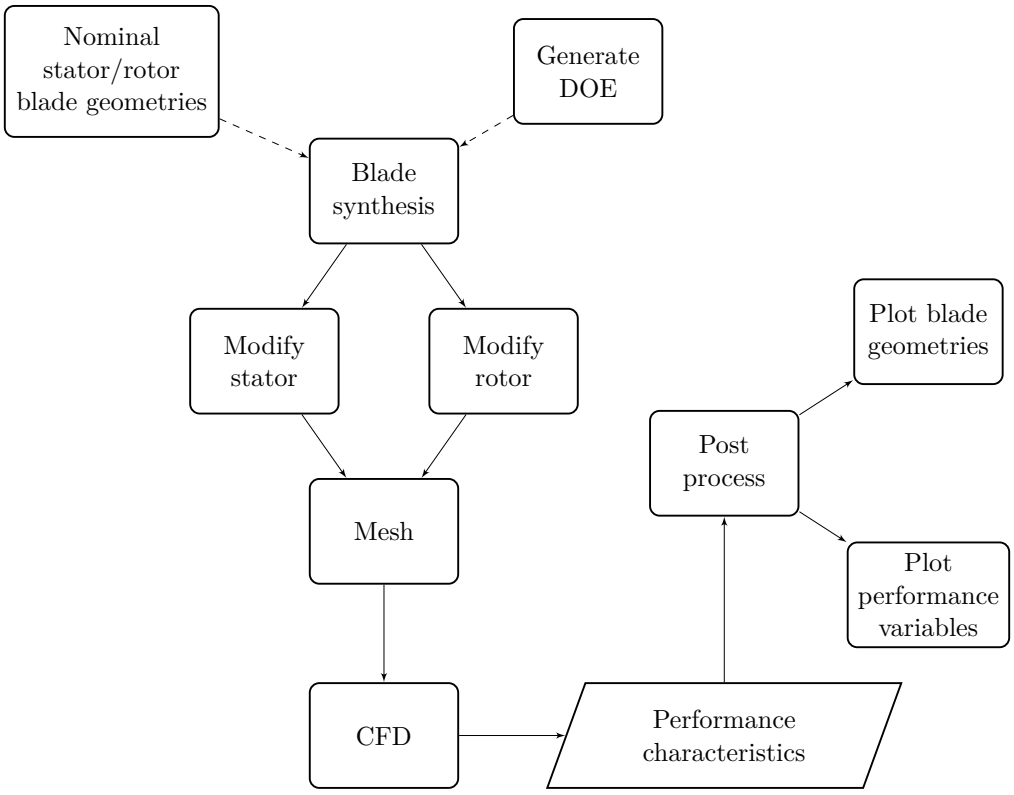

Figure 3.1: Infographic of 2LOOP, the method developed in this project used to synthesise turbine blades and analyse the impact of geometry variation on turbine performance.

3.2 Blade synthesis

In the milling process of turbine blades, manufacturing tolerances are defined in order to maintain cost efficiency. However, the permitted tolerances also mean that certain deviation from nominal design is bound to happen. While these variations are inherently random, it is of interest from a simulation perspective to have certain control of geometry variations when synthesising blades.

At GKN Aerospace, `PollyGraph` [11] is a blade design tool used for geometry generation of compressor and turbine blades. However, as mentioned, this project does cover design and generation of blades. Instead, 2LOOP presupposes that a blade geometry already exists, and proceeds to modify this geometry. The first stage of the project involved developing a method to synthesise manufacturing variations of these nominal blade profiles in order to generate a set of geometrically diverse blades. The blade generation files are stored in a specific data format which includes information on blade geometry, camber lines, and an axisymmetric flow path [12]. The blade geometry is divided into a number of sections in the spanwise (radial) direction, in which each section contains a point set of $x-$, $y-$ and $z-$coordinates, at constant span along the blade.

The point set for each section starts and ends at the trailing edge (TE). After that, the direction for the point set is clockwise as seen in a two-dimensional coordinate system defined by the $x-$ and $r\theta-$direction. Referring to Figure 3.2, the order of the point set then becomes TE $\rightarrow$ LS1 $\rightarrow$ LS0 $\rightarrow$ LE $\rightarrow$ US1 $\rightarrow$ US0 $\rightarrow$ TE. Consequently, the first and last point in the set is identical, i.e. the trailing edge point. Note that the order of the point set is also irrespective of the direction of the blade's suction and pressure sides. [12]

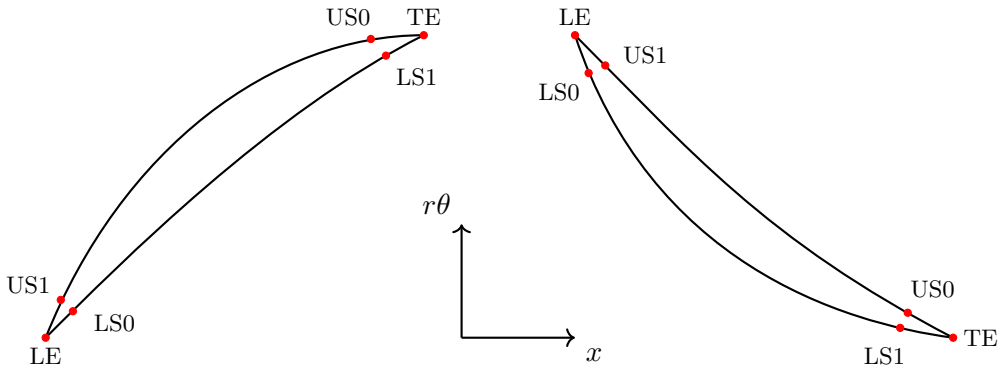

Figure 3.2: Points identifying leading and trailing edge for a section. Blade generation codes contain point sets for each section of the blade. Each point set in turn contains $x-$, $y-$, and $z-$coordinates for points describing the blade profile. The order of the point set is TE $\rightarrow$ LS1 $\rightarrow$ LS0 $\rightarrow$ LE $\rightarrow$ US1 $\rightarrow$ US0 $\rightarrow$ TE.

The blade profiles are modified using a sinusoid function whose maximum amplitude is limited by the profile tolerances. Blade geometry variations are then generated by varying the amplitude, period, and phase of the sinusoid. These variations are stored in the design tables. After the blades' geometries have been modified, the modified geometry coordinates are written to new format files, so as not to overwrite the nominal geometry. This way, a unique format file for each respective geometry variation contained within the design table is generated.

3.2.1 Sinusoidal profile variation

In order to modify the blade geometry to synthesise manufacturing variations, the blade profile coordinates are shifted in their respective normal direction within the tolerance band using a sinusoidal function. It should be noted that when referring to the tolerance it is the blade

profiles' shape tolerance that is considered. The shape tolerance is defined as the tolerance band around the nominal design (see Figure 3.3). When modifying the geometry of the blade, all points on the surface of the blade are kept within this tolerance band.

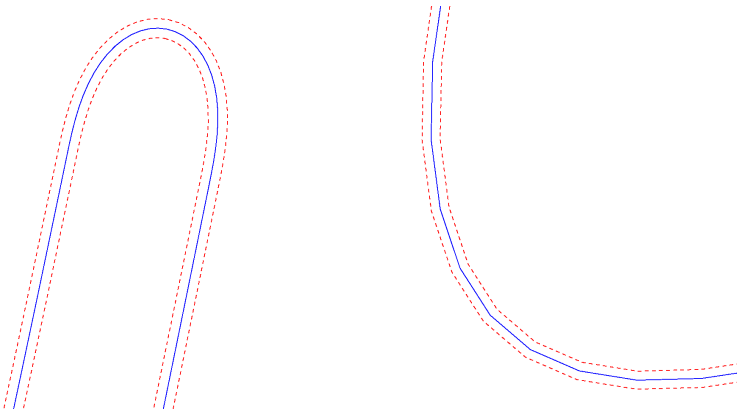

(a) Stator trailing edge **(b)** Rotor leading edge

Figure 3.3: Fragments of (a) stator and (b) rotor blade profiles, shown in blue. The dashed red lines represent the minimum and maximum values of the current tolerance band.

In order to define the sinusoid along the entire length of the blade profile, the length or circumference of the blade was first determined. The length from origin to a given point $i+1$ on the blade may be defined as

$$s_{i+1} = s_i + \sqrt{(x_i - x_{i+1})^2 + (y_i - y_{i+1})^2 + (z_i - z_{i+1})^2} \tag{3.1}$$

where s_i is the distance from the origin to the previous point, and the term within the square root represents the distance between the previous and the current point in terms of Cartesian coordinates. The index $i = 1, \ldots, N$ represents the points within the respective point sets in the format file. s_{i+1} is thus the distance from the origin to the current point being considered, As such, cycling through each point set results in the circumference of the blade, s_N. The circumference of the blade profile is in turn used to define a normalised blade length at every point i in the point set according to

$$s_{norm} = \frac{s_i}{s_N}$$

Figure 3.4 shows a fragment of an arbitrary blade profile. The points visualised represent those stored in the point sets as described. N such points make up the blade profile along the entire circumference of the blade, and represents one section of the blade. The blade geometry in its entirety is thus produced by extruding one such section in the radial direction. As mentioned in Section 3.2, the blade geometry is divided into a number of sections in the radial direction. Each section thus represents a slice of the blade, and each section is defined by its own point set with $x-$, $y-$ and $z-$coordinates along the profile.

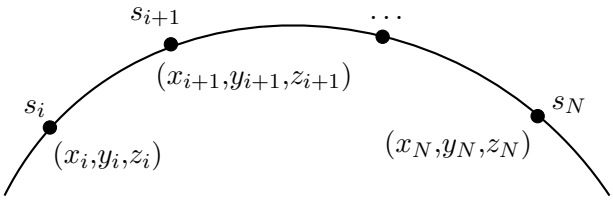

Figure 3.4: Fragment of an arbitrary blade profile. Each point is identified by its Cartesian coordinates (x,y,z) which are stored in the point set. s is the distance from origin to each respective point along the profile, as defined by Eq (3.1).

Due to the curved nature of the blisk (bladed disk) it is more intuitive to consider a polar coordinate system, in which the radius r_i at point i is defined as

$$r_i = \sqrt{y_i^2 + z_i^2}$$

As mentioned previously, each point set is defined for a constant radius along the blade span. The blade may then be considered in a two dimensional (2D) coordinate system defined by x and $r\theta$, where $r\theta_i$ at point i is defined as

$$r\theta_i = \sqrt{y_i^2 + z_i^2} \cdot \arctan\left(\frac{z_i}{y_i}\right) = r_i \cdot \arctan\left(\frac{z_i}{y_i}\right) \tag{3.2}$$

This allows the point set of each section in the file to be transformed to the $x-$ and $r\theta-$plane. In order to then shift the blade coordinates in the normal direction of each respective point in the point set, the $x-$ and $r\theta-$components of the unit tangent vector $\widehat{\mathbf{T}}$ for the segment between two adjacent points, i and $i+1$, are defined as

$$\widehat{\mathbf{T}}(x) = \frac{\Delta x}{\sqrt{(\Delta x)^2 + (\Delta r\theta)^2}} \qquad \widehat{\mathbf{T}}(r\theta) = \frac{\Delta(r\theta)}{\sqrt{(\Delta x)^2 + (\Delta r\theta)^2}}$$

where Δx and $\Delta r\theta$ is the distance in $x-$ and $r\theta-$direction, respectively, between adjacent points i and $i+1$. The unit point tangent vector of point i is computed by averaging the unit segment tangent vector between points $i-1$ and i and the unit segment tangent vector between points i and $i+1$, according to

$$\widehat{\mathbf{T}}_i(x) = \frac{\Delta\Big[\Delta(x)_{i+1} - \Delta(x)_i\Big]}{\sqrt{\Big(\Delta\Big[\Delta(x)_{i+1} - \Delta(x)_i\Big]\Big)^2 + \Big(\Delta\Big[\Delta(r\theta)_{i+1} - \Delta(r\theta)_i\Big]\Big)^2}}$$

$$\widehat{\mathbf{T}}_i(r\theta) = \frac{\Delta\Big[\Delta(r\theta)_{i+1} - \Delta(r\theta)_i\Big]}{\sqrt{\Big(\Delta\Big[\Delta(x)_{i+1} - \Delta(x)_i\Big]\Big)^2 + \Big(\Delta\Big[\Delta(r\theta)_{i+1} - \Delta(r\theta)_i\Big]\Big)^2}}$$

The modified blade profile is achieved by shifting the $x-$ and $r\theta-$coordinates of each point in the point set appropriately in their respective normal directions. Figures 3.5a and 3.5b show the unit point tangent and normal vectors for each point at the leading edge of the rotor.

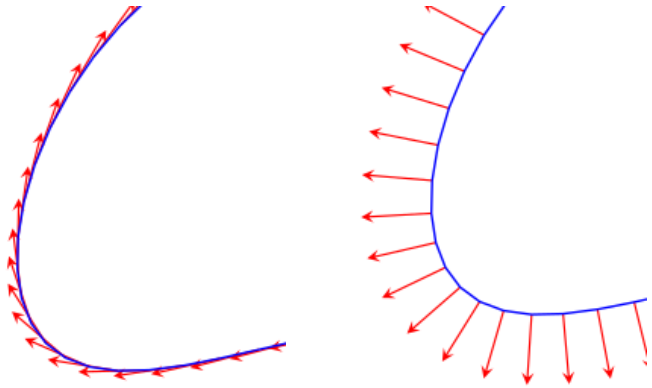

(a) Unit tangent vectors **(b)** Normal vectors

Figure 3.5: Tangent and normal vectors for a fragmented blade profile. When applying geometry variations to the blade profile, the points for each point set in the blade generation codes are shifted in the normal direction.

The modified blade profile used in the simulations is achieved by shifting the $x-$ and $r\theta-$coordinates of each point in the point set appropriately in their respective normal directions with a sinusoidal function $f_{\sin}$, such as

$$f_{\sin}(A_i, n_i, \varphi_i) = A_i \cdot \sin\left(2\pi n_i \cdot s_{norm} + \frac{\varphi_i \pi}{180}\right) \tag{3.3}$$

where A_i is the amplitude of the sinusoid, n_i is the period, and φ_i is the phase angle. The index i references to whether the stator s or rotor r is being altered, as these are modified separately. Utilising the sinusoidal function, the modified $x-$ and $r\theta-$coordinates at each point are given by

$$\begin{aligned} x_{i,sin} &= x_i + f_{\sin} \cdot \left(-\widehat{\mathbf{T}}_i(r\theta)\right) \\ r\theta_{i,sin} &= r\theta_i + f_{\sin} \cdot \left(\widehat{\mathbf{T}}_i(x)\right) \end{aligned}$$

Finally, the modified coordinates are then transformed back to the xyz-plane according to

$$\begin{aligned} y_i =& r_i \cdot \cos\theta_i = r_i \cdot \cos\left(\frac{r\theta_i}{r_i}\right) \\ z_i =& r_i \cdot \sin\theta_i = r_i \cdot \sin\left(\frac{r\theta_i}{r_i}\right) \end{aligned}$$

As manufacturing noise is seemingly random and hard to predict, it was of interest to develop a method to geometric variability. While a sinusoid variation may not perfectly emulate reality in terms of manufacturing variations, it gives the user three distinct parameters (amplitude A_i, period n_i, and phase angle φ_i) to vary in order to analyse the impact of geometric variability in a relatively simple manner. Although the synthesised variations generated by the sinusoid are perhaps not entirely random, it may give insight as to the effect of geometry variability within current profile tolerances. The sinusoid provides control over geometry variations between design cases, allowing easier follow-up on which variations that source a certain scatter in performance, as opposed to if a more random function was employed. This may also aid in future efforts regarding both tolerance and geometry design.

3.3 Design cases and DOE generation

A number of different design cases have been considered during this project, which have each required a unique design table containing variations of amplitude, period, and phase angle for the sinusoidal function used to modify blade geometry. The design tables are stored in text files to be read by the Python programs. While the design table is unique for each design case, the structure of the design table is identical whereby each entry contains an ID number for identification, as well as values for amplitude (A_s, A_r), period (n_s, n_r), and phase angle (φ_s, φ_r) for both the stator (s) and rotor (r), respectively.

Due to confidentiality, actual blade geometry values and tolerances are withheld, including values of the amplitudes for the stator and rotor, A_s and A_r respectively, as these values correspond to the profile tolerances. Thus, these will instead be referred to as “maximum” and “minimum” to identify when the maximum and minimum tolerance values are applied. Nominal amplitude is concurrent with a value of zero, such that the sinusoidal function in Eq (3.3) vanishes. The different DOE cases generated and analysed are further described below.

3.3.1 Profile tolerances

For profile tolerances design, geometry variation involved modifying the blade profile surface points to assume the minimum and maximum values of profile tolerance band. These profile variations were obtained with the sinusoid function $f_{\sin}$ (Eq (3.3)) by setting the period and phase angle of the sinusoid to zero and 90°, for which the sinusoid assumes unity. The amplitude A_i was then varied between nominal amplitude (nought), and maximum and minimum tolerance values. This resulted in three variations of stator and rotor blades, respectively, and a total of five configurations that were simulated. The profile tolerance design table is shown in Table A.1 in Appendix A. These provided an initial estimation of the effects of geometric variability on performance with a relatively simple modification to the blade profile.

3.3.2 Latin hypercube design

In the Latin hypercube design case, the amplitude of the sinusoid was kept constant and equal to the maximum profile tolerance such that the peaks of sinusoidal function oscillated between the maximum and minimum profile tolerance. Hence only the period and phase angle are varied for each configuration. These variations were generated based on Latin hypercube sampling as introduced in Section 2.2.1. The Latin hypercube sampling was generated using a Python code which takes the number of factors to generate samples for (m), and the number of samples to generate for each factor (p) as input, and returns an m-by-p design matrix (H) [13]. However, the values in the design matrix H have been normalised so that the factor values are uniformly spaced between zero and one. When the LHS matrix was generated for the LHS design case, the number of factors was set to $m = 4$ (n_s, n_r, φ_s, φ_r) while the number of samples for each factor was set to $s = 100$ which resulted in a 4-by-100 design matrix with values uniformly distributed between zero and unity.

As the sampled values are intended as input variables to the sinusoidal function, they first need to be reshaped in order to meet the physicality of a sinusoid. The sampled period values were multiplied by a factor 10 and shifted so that the period was uniformly distributed between 1 and 10. The phase angle values, on the other hand, were multiplied by a factor of 360, and thus uniformly distributed between 0° and 360°. However, as the values were initially uniformly distributed between zero and unity, simply multiplying these by a factor results in non-integer values of both the period and phase angle, which is not feasible. Therefore, the values were then rounded to the nearest integer, which resulted in the possibility of values being sampled more than once (for example, both 0.68 and 0.83 round to 1). Recalling the conditions of a Latin hypercube from Section 2.2.1, the resulting design matrix was, strictly speaking, not a Latin hypercube. It should however be noted that, while a specific variable may be sampled more than once, a specific combination of stator-rotor variables, or configuration, was not. For this reason, the design matrix consisted of 100 unique configurations of blade geometry variations to be performed.

3.3.3 Phase angle variation

In the phase angle variation design case, two separate cases were generated in which only the phase angle was varied; one for which the stator's profile was kept at nominal design while only the rotor's phase angle was varied, and one for which the rotor's profile was kept at nominal design while only the stator's phase angle was varied. This was done in order to determine which of the blades had greatest impact on performance when exposed to geometry variations, as well as if there were any regions on along the blades' profiles that were more or less sensitive to manufacturing variability.

As mentioned in Section 3.2, the point set for each section starts and ends with the trailing edge point. When applying the phase angle variation, this essentially dictated how far from the trailing edge point that the sinusoid was shifted. This is visualised in Figure 3.6 where the solid (red) line represents an unshifted sinusoid, the dashed (black) line a sinusoid that has been shifted by some $\varphi \neq 0$, and origo the trailing edge point of the blade.

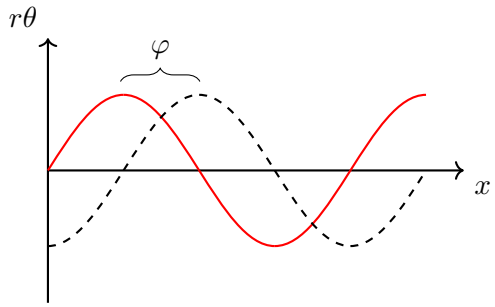

Figure 3.6: Visualisation of phase angle variation along the blade profile. The solid (red) line represents an unshifted sinusoid ($\varphi = 0$) while the dashed (black) line represents a sinusoid shifted by some $\varphi \neq 0$. The shift is relative to origo, which represents the blade trailing edge point. Both sinusoids visualised here have the same amplitude and period.

The phase angle variation was done in increments of 15° in the range of 0° to 360° which yielded 25 unique configurations to be simulated. For these cases, the amplitude was again kept constant and equal to the maximum profile tolerance, while the period was kept constant and equal to $n_i = 1$ in order to focus on the impact of the phase angle. These two design cases were then repeated but with a constant period of $n_i = 2$. Other than this, all of the other parameters were kept the same. The design tables for the phase angle variation cases are shown in Tables A.3-A.6 in Appendix A.

3.3.4 Summary of design cases

Table 3.1 shows an overview of the different design cases carried out in the project as described in Sections 3.3.1-3.3.3, as well as the number of blade configurations generated, meshed, and simulated. Design tables for the respective design cases can be found in Appendix A.

Table 3.1: Summary of the different design cases implemented in the project and the number of stator-rotor configurations for each of the design cases.

DOE#	Description	Number of configurations
1	Profile tolerances – amplitude is varied between nominal (nought), minimum and maximum tolerance values	5
2	Latin hypercube design – values for period n_i and phase angle φ are generated with LHS script	100
3	Rotor phase angle variation – phase angle for rotor φ_r is varied with degree increments of 15°, single period ($n_r = 1$) - nominal stator design	25
4	Stator phase angle variation – phase angle for stator φ_s is varied with degree increments of 15°, single period ($n_s = 1$) - nominal rotor design	25
5	Rotor phase angle variation – phase angle for rotor φ_r is varied with degree increments of 15°, dual period ($n_r = 2$) - nominal stator design	25
3	Stator phase angle variation – phase angle for stator φ_s is varied with degree increments of 15°, dual period ($n_s = 2$) - nominal stator design	25

3.4 Meshing

Meshing was performed using an in-house developed structured multi-block grid generator, known as `G3dMesh`. `G3dMesh` is a Fortran code and uses the point set data described in 3.2, as well as input mesh parameters which may be edited by the user. Meshes generated by `G3dMesh` are so-called "block-structured meshes" (as opposed to unstructured meshes). Generally, structured meshes have better numerical properties compared to unstructured meshes, resulting in higher resolution and better convergence [8].

A block-structured grid divides the mesh domain into different regions and while each region has a structured mesh, the actual structure from region to region may be defined separately. This gives block-structured grids the advantage of higher flexibility as the user may refine the mesh in certain critical areas, while retaining a lower resolution in other, less critical areas [14]. `Meshblade` is a parametrised input file to `G3dMesh`, which supports three predefine topologies, where topology refers to block connectivity, orientation, and outline of the blocks. Figure 3.7 shows approximate outlines for the three supported topologies and the difference in blocking between these. When running the grid generator, the default topology is H-grid (3.7a). If an alternate topology is desired, such as quarter o-grid out or quarter o-grid in (3.7b and 3.7c, respectively) this must be defined by the user as an input parameter when running the mesh script. [15]

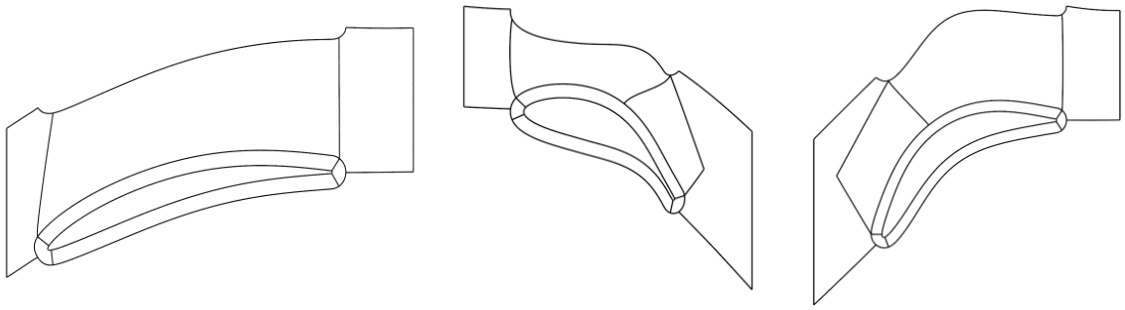

(a) H-grid **(b)** Quarter o-grid out (qoo) **(c)** Quarter o-grid in (qoi)

Figure 3.7: Supported topologies by the meshing routines in in-house codes and shell scripts. Topology is set as a parameter when the meshing script is started, where H-grid (3.7a) is the default topology, and used to define the number of blocks and nodes within the respective blocks. Courtesy of GKN Aerospace [15].

Due to the difference in geometry and stagger angles of the stator and rotor rows, these require different topologies. Therefore, the stator and rotor blades are meshed and refined separately.

As a large number of combinations of geometry variations were to be simulated, it was of interest to automate the process as much as possible. In order to to this, a mesh template was generated for the stator and rotor, respectively. The mesh template was obtained by meshing and refining the the blades' respective nominal geometries until the quality of the mesh was deemed sufficient. Mesh quality was assessed mainly in terms of the Jacobian, where best practice values at GKN Aerospace were used as target values as well as visual evaluation of the mesh to ensure that no cells appear to be excessively stretched or warped. Mesh refinement was done by varying values for the number of nodes on the suction and pressure sides, number of nodes at the leading and trailing edges, and node spacing. Inner and outer o-grid node spacing as well as the number of nodes in different directions for the various blocks were also adjusted during the refinement process. When the quality was satisfactory, the mesh templates could then be used for subsequent meshing of the blades prescribed in the respective DOE design tables as it was assumed that the geometry variations are relatively small in scale compared to the blade geometry as a whole, and do not impact mesh settings or quality markedly. This was then determined as the Jacobian did not vary between meshes.

A plenum was also added at the outlet of the rotor for simulation purposes in order to evaluate the flow slightly downstream of the the rotor trailing edge. By evaluating the flow downstream of the trailing edge, the flow profile is given time to develop and stabilise, providing a better description of the flow.

Templates for the stator, rotor and plenum are written to file and stored. As such, when the main script of 2LOOP is executed, meshing of the blades is done automatically for each configuration in the design table by using the mesh templates for the stator and rotor, respectively. The generated grids are assembled in a mesh for the entire stage and written to file to be used for the CFD simulations.

3.5 CFD simulations

CFD simulations are performed using `VolSol++`, an in-house block-structured, compressible Navier-Stokes solver written in C++, which uses a text-based solver input [16, 17]. As with the meshing process, a general solver input template is generated and used to create a unique input for each configuration to be simulated.

The solver input template contains data concerning the mesh, such as mesh block connectivity and rotational periodic block interfaces. Mesh block connectivity refers to, as the name suggests, how two blocks are connected and is determined by defining two 'faces' which are to be connected. Faces are defined by their block number, starting position, the mesh directions of the face, as well as the number of points or nodes in each direction [17]. Rotational periodic block interfaces are defined in a similar manner, with the addition of a rotation angle for both of the faces which determines the period of the face.

As the entire stage was simulated, this essentially created two flow domains, one for each of the components. In order to couple the simulation information between the respective domains, a mixing plane model was employed between the stator and rotor. Flow property profiles at the stator outlet can then be used at the rotor inlet and continuity over the flow domains is maintained. A mixing plane was also defined between the rotor outlet and the plenum's inlet in order to maintain continuity over this interface as well.

Aside from general settings for the CFD simulations, the solver input template also includes specification of which variables to monitor and output, as well as case-specific data. The turbine considered was simulated and evaluated for two different qualification points, which represent different operating conditions of the turbine in terms of certain parameters, such as inlet temperature, inlet mass flow, and rotational speed, to name a few. The two qualification points considered are referred to as Reference Operating Conditions (ROC) and Q4. Normalised data for these operating conditions are shown in Table 3.2.

Table 3.2: Operating conditions for different qualification points for which the turbine has been evaluated for. Note that data has been normalised relative to the reference operating conditions (ROC).

Parameter	Variable	Qualification point	
		ROC	Q4
Inlet total temperature	$T_{0,in}$	1.0	1.04
Inlet total pressure	$P_{0,in}$	1.0	0.80
Outlet total pressure	$P_{0,out}$	1.0	0.88
Total pressure ratio	Π	1.0	0.91
Inlet mass flow	$\dot{m}_{in}$	1.0	0.78
Rotational speed	N	1.0	0.89

The data for the respective qualification points are stored in a configuration file parser or `ConfigParser`. The structure of the `ConfigParser` allows it to be read by the main script and, depending on which qualification point was being considered, substitute certain data in the solver input template with the according data. This way, 2LOOP can easily be modified if alternate qualification points are to be investigated. All of the design cases described in Section 3.3 were simulated for both of the qualification points.

It should be noted that the terms *qualification point* and *operation conditions* are equivalent. Both terms are used interchangeably throughout the report and the reader should be aware that these refer to the same concept.

3.5.1 Simulation cases

A separate simulation case was generated for each respective design case defined in Section 3.3. For the initial profile tolerance design case (see Section 3.3.1), simulations were done for eight different pressure ratios ranging from 1.1 to 3 for each configuration and each qualification point, which resulted in a total of 16 simulations per configuration for a total of 80 simulations in this initial design case. This was done in order to generate a turbine map, i.e. the flow function Q against the pressure ratio Π. The turbine map is a set of speed lines for the same corrected speed showing the range of variation in performance for the configurations listed in Table A.1 – one speed line for each configuration. An exemplary turbine map can be seen in Figure 3.8 where flow function Q is plotted against total pressure ratio Π.

The obtained turbine map and a speed line analysis of the nominal design results were used to adjust inlet and outlet conditions to the point in the turbine map that best corresponds to the operating conditions prescribed for the respective qualification points as listed in Table 3.2. As such, subsequent simulation cases are done for only one pressure ratio, rather than the previous eight pressure ratios, which results in only two simulations per configuration (compared to the previous 16). The predicted scatter of the subsequent DOE cases is also visualised in Figure 3.8, and as can be seen it was predicted that the scattering fall within the speed lines corresponding to maximum-maximum and minimum-minimum configurations of stator-rotor geometries.

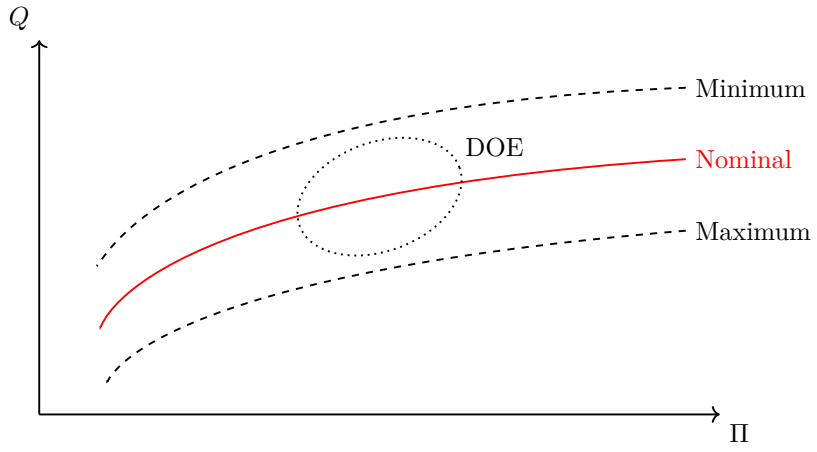

Figure 3.8: Exemplary turbine map of the profile tolerance case and predicted scattering of subsequent DOE configurations. The solid (red) speedline represents nominal-nominal stator-rotor design, while the dashed (black) lines represent maximum-maximum and minimum-minimum configurations. The dotted region represents the predicted scattering as a result of geometry variations in the various design cases.

Apart from the the different configurations and design cases, there were no other differences between the simulation models. The initial design case was simulated for 25 000 iterations, while subsequent simulations were done for 15 000 iterations as it was seen that this was enough

for simulations to converge. Convergence was considered with respect to when the residuals appeared to level off. It should be noted, however, that even though a residual has levelled off, there may still be some fluctuations in the solution that must be accounted for, and are taken into consideration when post-processing the results.

3.6 Post-processing

`VolSol++` outputs simulation results to a series of logs and text files to be interpreted and processed by the user, including monitor values for variables-of-interest pre-defined by the user for each iteration. Variables-of-interest for this project include mass-averaged values of stagnation pressure and temperature, static pressure and temperature, as well as the mass flow, all of which are recorded at both the inlet and outlet of the stage.

Once simulations are completed, 2LOOP's post-processing is initiated. The post script retrieves monitor values for each iteration of the simulations and stores these values for post processing. Post processing calculations are performed, in which the efficiency η and non-dimensional flow function Q are calculated according to equations (2.3) and (2.4), as well as the pressure ratio according to (2.6). As mentioned in Section 3.5.1, converged solutions may have some small-scale fluctuations between iterations. In order to account for this fluctuation, the post-processed results are averaged over the last 1000 iterations. The averaged results are then normalised with respect to simulation results for nominal design conditions (in terms of blade geometry) and reference operating conditions, due to confidentiality. The post-processed, averaged data is written to file and used in subsequent scripts for plotting and analysing the results. Performance plots for the parameters-of-interest are generated, along with profile plots of the blade profiles for the efficiency extremes observed in each respective design case in order to investigate any geometry variation trends that may affect performance.

4

Results and Discussion

In the following chapter, the main results of the project are presented and discussed. The chapter is divided into three parts; the first concerning the results regarding the method development, while the second concerning the results of the method implementation and evaluation. The results for the respective simulation cases are analysed and discussed to provide some insight as to the results and phenomena observed. Due to confidentiality, simulation results are normalised with respect to simulation results for nominal blade designs and reference operating conditions. Finally, a review of the impact of blade tolerances on turbine performance is presented.

4.1 2LOOP

The principal result of this project is the development of a method with the possibility of studying the impact of manufacturing tolerances on turbine performance. It is important to note, however, that 2LOOP is not a fully automated loop, and is also not a loop intended for blade optimisation. Instead, it is a method developed for synthesising turbine blades with geometric variability as a means of replicating manufacturing deviations from nominal blade design.

2LOOP in its current state allows the user to analyse effects on turbine performance when turbine blades vary from nominal design within given manufacturing tolerances. Within the scope of this thesis, the geometric variability applied to turbine blades has been limited to those produced by a sinusoidal function, as presented in Section 3.2.1. However, as shown in the various design cases presented in Section 3.3, the sinusoidal function shows versatility, allowing for a multitude of geometry variations. 2LOOP also allows for multiple qualification points to be considered and analysed simultaneously. Consequently, turbine performance may be analysed for various operating conditions in order to determine the impact of geometry variations over a range of operating conditions, which may aid in future blade and tolerance design.

While a sinusoidal profile variation may not be realistic in every respect or a completely accurate representation of actual manufacturing variations, it provides an acceptable initial implementation of profile variations and the implications of these on turbine performance. The sinusoidal profile variation is representative to study the impact of blade tolerances on turbine performance as it produces near-random geometry variability of blade profiles within the manufacturing profile tolerances. The benefit of a sinusoidal profile variation allows for simple modification in future implementations, which introduces the possibility of analysing other, perhaps more realistic variations such as a those visualised in Figure 4.1. Other options may involve limiting geometry variations to only certain parts along the blade profile. This may provide better insight and understanding of which parts along the blade profile that are most sensitive to geometry variations, which may make it feasible in introducing different design tolerances along the profile.

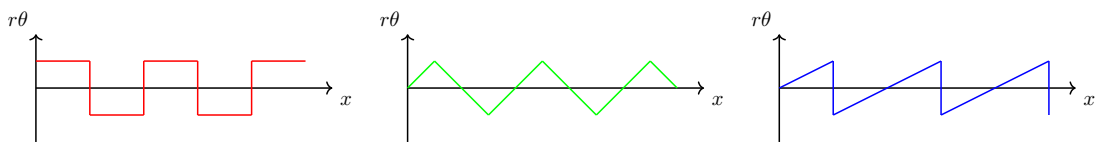

(a) Square **(b)** Triangle **(c)** Sawtooth

Figure 4.1: Potential sinusoid variations which may be implemented in future versions of 2LOOP.

Furthermore, while the profile variations considered in this projected have been limited to current manufacturing tolerances set upon the stator and rotor blades, it does not limit future studies of blade profiles exceeding these manufacturing tolerances. Future implementation may for example see a fusion of theLOOP and 2LOOP, making it possible to optimise blade profiles as well as manufacturing tolerances. An optimisation of the tolerances may lead to more robust designs as well as improved cost efficiency in the manufacturing processes.

4.2 Simulations results

In the following sections, simulation results from the various design cases outlined in Section 3.3 are presented. Some discussion as to observations made of the results are presented in conjunction with this. The simulations were performed as per the methodology described in Section 3.5 and post-processing as per Section 3.6.

4.2.1 Profile tolerances

The first design case consisted of five configurations where blade design for the stator and rotor was varied between nominal design and the minimum and maximum profile tolerance limits as described in Section 3.3.1. Figure 4.2 shows the simple geometry variations of both the stator and rotor profiles that were considered in the initial profile tolerance design case

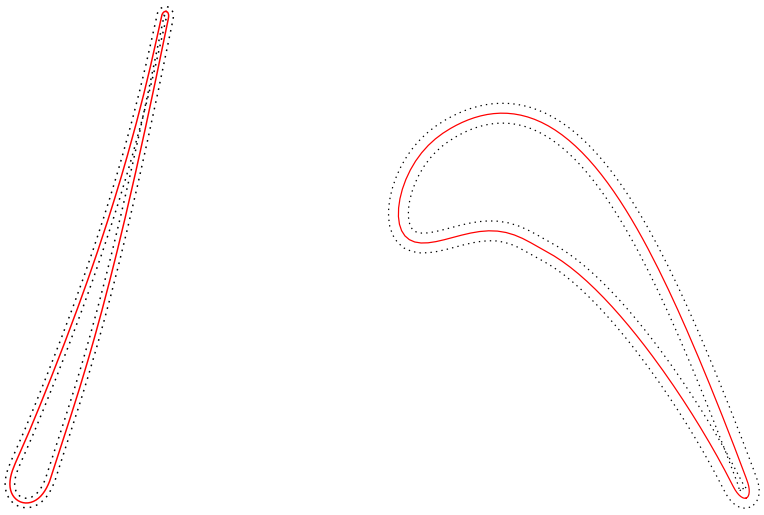

(a) Stator profile **(b)** Rotor profile

Figure 4.2: Geometry variations considered in the profile tolerance design case. The dotted (black) lines represent the profile tolerances, while the solid (red) line represents nominal design. It should be noted that the blade geometries are not to scale, and also that the profile tolerance band has been magnified for better visualisation.

Simulation results were post processed and turbine maps for the flow function Q versus pressure ratio Π for the respective qualification points were generated. Figure 4.3 shows the flow function Q versus pressure ratio Π for the two operating conditions. As can be seen, the flow function increases with increased pressure ratio across the turbine, until a certain point where the flow function reaches a maximum where the stage becomes choked. If the value of the flow function at choked conditions is the same for all speeds, then it is a sign that the stator is choked. If the rotor is choked, the value of the flow function instead varies with rotational speed.

Further, it can be seen that the speed lines for the stator-rotor configurations for minimum-minimum and maximum-maximum profile tolerance result in the boundaries, with speed lines for maximum-minimum and minimum-maximum configurations falling within these boundaries.

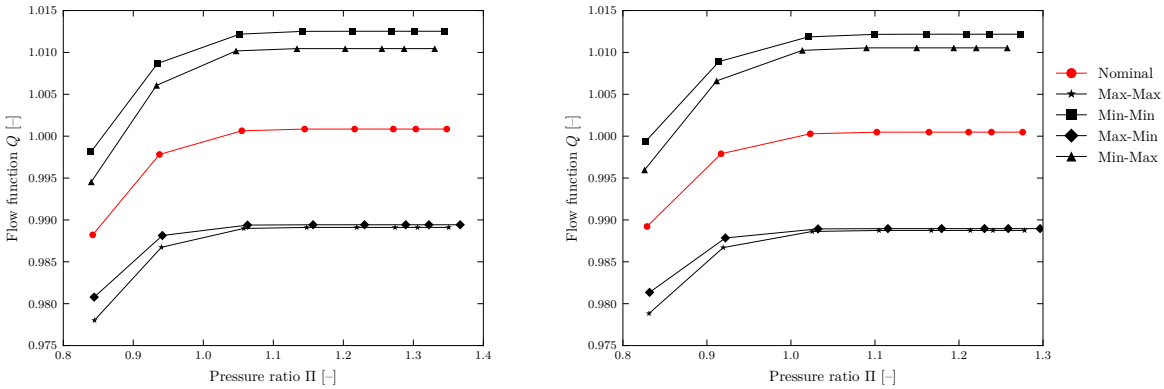

(a) ROC **(b)** Q4

Figure 4.3: Turbine maps of flow function Q versus pressure ratio Π for (a) ROC and (b) Q4 for the profile tolerance case in which blade profiles were varied between nominal, minimum and maximum profile. Results are normalised relative to results for nominal blade design and ROC.

Figure 4.4 shows the efficiency η versus pressure ratio Π for the respective operating conditions. Here it can be seen that the efficiency in general decreases with increased pressure ratio, except for a local maxima which appears for (normalised) pressure ratios in the range $\Pi = 1.15 - 1.3$, depending on the operating conditions and stator-rotor configuration. Similar to the flow function, the efficiency appears to level off, although without results for higher pressure ratios, this cannot be said for certain.

It should also be noted that the limiting curves for efficiency are characterised by the stator-rotor configurations corresponding to maximum-minimum and minimum-maximum profile tolerances, as opposed to the maximum-maximum and minimum-minimum configurations as for the case of flow function against pressure ratio (see Figure 4.3).

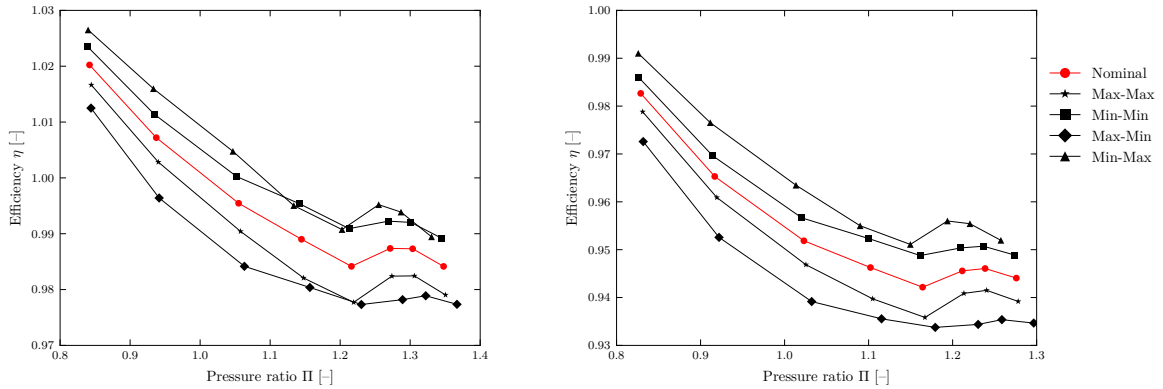

(a) ROC **(b)** Q4

Figure 4.4: Turbine maps of efficiency η versus pressure ratio Π for (a) ROC and (b) Q4 for the profile tolerance case in which blade profiles were varied between nominal, minimum and maximum profile. Results are normalised relative to results for nominal blade design and ROC.

Figures 4.3 and 4.4, and subsequent figures, contain line segments between discrete points representing results from separate simulations, however it cannot be assumed that future simulations between these points will be described accurately by the respective line segments in this graphs. The line segments represent a linear interpolation between computed operating points. It is assumed that these line segments capture the trend of these simulations, and that future simulations should fall somewhere in the vicinity of the respective segments, although this can of course not be said for certain without a larger data set of simulations.

4.2.2 Latin hypercube design

The second design case simulated was the Latin hypercube design as described in 3.3.2. The resulting design matrix of period and phase angle variations from the Latin hypercube script that was used as the design table for the second design case is shown in Table A.2 in Appendix A.

Figure 4.5 shows turbine maps for the flow function Q versus pressure ratio Π for the respective qualification points. Included in these graphs are the results from the 100 configurations in this design case. As can be seen, the scatter of DOE results fall within the boundaries defined by the stator-rotor configurations for minimum-minimum and maximum-maximum profile tolerance as predicted. As mentioned in Section 3.5.1, the simulation set up for all subsequent design cases after the initial case were done for only one pressure ratio. The resulting DOE scatter therefore has limited variation in terms of pressure ratio and are concentrated around the same pressure ratio as seen in Figure 4.5.

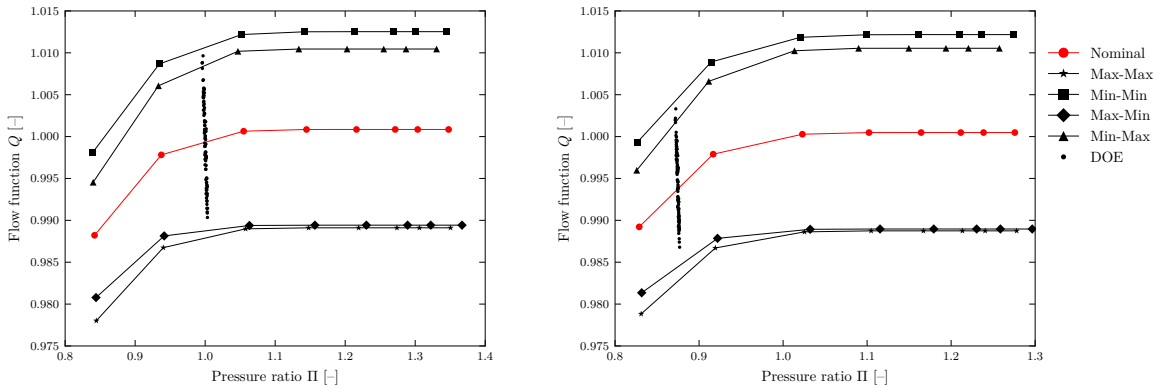

(a) ROC **(b)** Q4

Figure 4.5: Turbine maps of flow function Q versus pressure ratio Π for (a) ROC and (b) Q4 for which blade profiles were modified with the sinusoidal function $f_{\sin}$. Values for phase angle and period were generated through Latin hypercube sampling. Results are normalised relative to results for nominal blade design and ROC.

Figure 4.6 shows the efficiency η versus pressure ratio Π for the respective operating conditions, as well as included in these graphs are the results from the 100 configurations in this design case. Similar to the results for flow function versus pressure ratio, the DOE scatter for efficiency also fall within the boundaries from the initial design case, with a few exceptions for certain configurations simulated with ROC, which represent the outliers are are seen in Figure 4.6a. As mentioned in Section 4.2.1, however, the boundaries made up of the line segments are only linear interpolations between the computed operating points, thus it can be argued that these outliers may not in fact be outliers as the it cannot be said for certain what the conditions between two points of any given line segment actually look like.

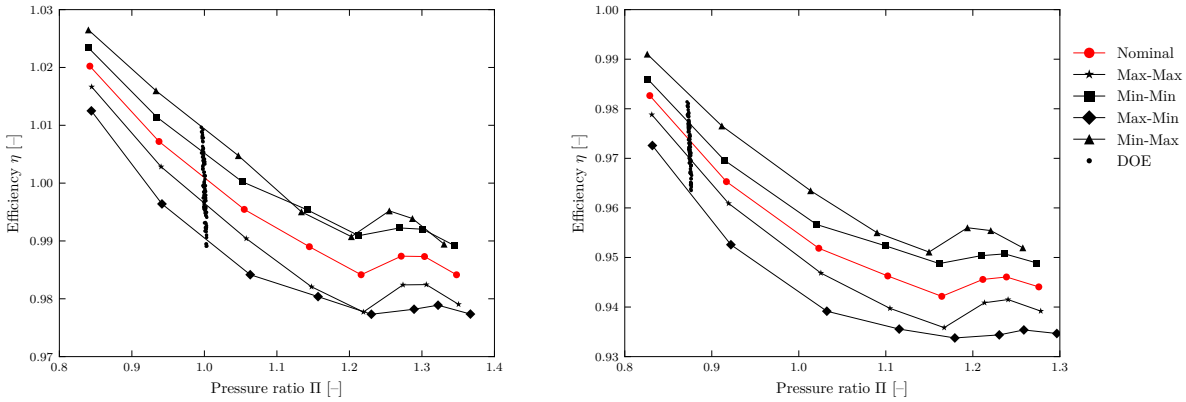

(a) ROC **(b)** Q4

Figure 4.6: Turbine maps of efficiency η versus pressure ratio Π for (a) ROC and (b) Q4 for which blade profiles were modified with the sinusoidal function $f_{\sin}$. Values for phase angle and period were generated through Latin hypercube sampling. Results are normalised relative to results for nominal blade design and ROC.

In order to determine if there were any characteristic traits in geometry variation that could explain the variation in efficiency, the blade profiles for the configurations resulting in the minimum and maximum efficiencies were plotted. It was found that the configurations that produced the minimum and maximum efficiency, respectively, was irrespective of the qualification point.

Figure 4.7 shows the stator profiles that resulted in minimum (4.7a) and maximum (4.7b) efficiency, respectively. Minimum efficiency was achieved for the stator configuration with period $n_s = 9$ and phase angle $\varphi_s = 59.0°$, while maximum efficiency was achieved for the stator configuration with period $n_s = 3$ and phase angle $\varphi_s = 259.0°$ (this corresponds to ID22 and ID76 respectively in Table A.2 in Appendix A). As can be seen in Figure 4.7, the stator profile for minimum efficiency is markedly less smooth than the profile for maximum efficiency, which is simply a result of the period being three times greater for the profile with minimum efficiency than that for maximum efficiency. Furthermore, the profile on the left (minimum efficiency) appears to have a thicker trailing edge, around maximum profile tolerance at the trailing edge, as opposed to the profile for maximum efficiency, which falls somewhere between minimum profile tolerance and nominal design. This is most likely a result of the phase angle, as the shift in phase angle determines where the peaks from center of the sinusoid occur. The smoother profile and thinner trailing edge may result in a smoother fluid flow around the stator, which results in improved inlet conditions for the rotor, and contributes to lower losses and an overall increased efficiency.

Note in Figure 4.7a that the stator appears to be exceptionally narrow at certain areas, which may seem infeasible. This exceptional narrowness is simply a result of magnifying the geometry variations and as such does not represent reality.

Figure 4.7: Stator profiles for (a) minimum and (b) maximum efficiency obtained in the Latin hypercube design case. The profiles for the respective qualification points, ROC and Q4, are identical as minimum and maximum efficiency occurs for the same configurations for both qualification points. The solid (red) line represents nominal design, while the dotted (black) lines outline the profile tolerances. Note that geometry variations have been magnified for better visualisation.

Figure 4.8 shows on the other hand the corresponding rotor profiles that resulted in minimum (4.8a) and maximum (4.8b) efficiency, respectively. Minimum efficiency was achieved for the rotor configuration with period $n_r = 3$ and phase angle $\varphi_r = 51.0°$, while maximum efficiency was achieved for the rotor configuration with period $n_r = 2$ and phase angle $\varphi_r = 256.0°$ (this corresponds to ID22 and ID76 respectively in Table A.2 in Appendix A). As opposed to the stator profiles, the rotor profiles do not differ greatly in period ($n_r = 3$ for minimum efficiency as opposed to $n_r = 2$ for maximum efficiency), making it more challenging in discerning the importance of period on performance.

However, similar to the stator profile, the rotor profiles also give evidence as to the effect of trailing edge thickness on efficiency. This can be seen in Figure 4.8b having a much sharper trailing edge, resulting in maximum efficiency, as opposed to the rounder, thicker trailing edge in Figure 4.8a, resulting in minimum efficiency. The profile on the right (4.8b) also appears to have a somewhat sharper leading edge, as well as a profile with a more gentle slope from leading to trailing edge.

Note in Figure 4.8b that the rotor's suction and pressure sides appear to cross over one another near the trailing edge of the blade. Again, this is merely due to the fact that the geometry variations have been magnified such that the magnified profile variations cross.

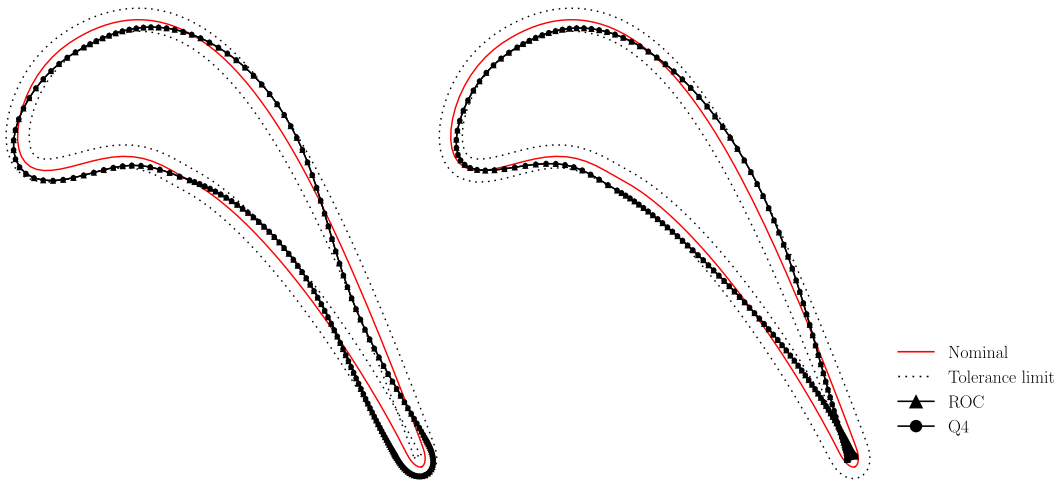

Figure 4.8: Rotor profiles for (a) minimum and (b) maximum efficiency obtained in the Latin hypercube design case. The profiles for the respective qualification points, ROC and Q4, are identical as minimum and maximum efficiency occurs for the same configurations for both qualification points. The solid (red) line represents nominal design, while the dotted (black) lines outline the profile tolerances. Note that geometry variations have been magnified for better visualisation.

Table 4.1 shows an overview of the results for the latin hypercube design in terms of the configurations resulting in maximum and minimum efficiency, η_{max} and η_{min}, respectively. Also listed in the table are the corresponding values of the flow function for the configurations resulting in maximum and minimum efficiency. Although flow function appears to trend with efficiency, it should be pointed out that these values are *not* the global maximum and minimum values of flow function, i.e. maximum flow function does result in maximum efficiency, and vice versa. The same is true for the minimum values.

Table 4.1: Summary of Latin hypercube results showing normalised values of η_{min} and η_{max}, as well as corresponding normalised values of the flow function. Results are normalised against results for nominal blade design simulated with ROC.

Qualification point	η_{min}	η_{max}	Q_{min}	Q_{max}
ROC	0.9891	1.0097	0.9923	1.0088
Q4	0.9635	0.9814	0.9889	1.0020

As the latin hypercube design produces variations of both period n_i and phase angle φ_i for stator and rotor profiles simultaneously, it is difficult to determine which parameters impact turbine performance, in terms of efficiency and flow function, most significantly. In order to test the robustness of these results, it was determined that a sensitivity analysis was necessary, whereby only one of the blades would be modified at a time. Furthermore, this sensitivity analysis was conducted by varying only the phase angle, while the period was kept constant. This was done in order to focus on the impact of the phase angle as mentioned in Section 3.3.3.

4.2.3 Phase angle variation

As mentioned in Section 4.2.2, the results from the latin hypercube design were used as basis for the phase angle variation design cases. Two design cases were generated in order to investigate which of the blades impacted performance most significantly; one design case in which the stator profile remained unaltered, while varying rotor phase angle, and one design case in which the rotor profile instead remained unaltered while varying stator phase angle. As mentioned, the

phase angle varied between $0 - 360°$ with a $15°$ interval between variations. The design tables for these design cases are shown in Tables A.3 and A.4, respectively (see Appendix A). The period was kept constant and equal to $n_i = 1$.

After the two initial phase angle variation cases were done, two further design cases involving phase angle variation were generated. These cases differed from the initial cases by setting the period of the blade being modified constant and equal to $n_i = 2$ (recall that only one blade was modified while the other remained unaltered). The design tables for these cases are presented in Tables A.5 and A.6.

4.2.3.1 Single period

Figure 4.9 shows the turbine map of flow function Q versus pressure ratio Π for the two phase angle variation cases where the period was set to unity (n_i). Figure 4.9a show the performance scatter when the rotor phase angle was varied, while Figure 4.9b instead show the scatter when the stator phase angle was varied. As can be seen, varying stator phase angle produces a greater variation in terms of flow function as opposed to varying rotor phase angle.

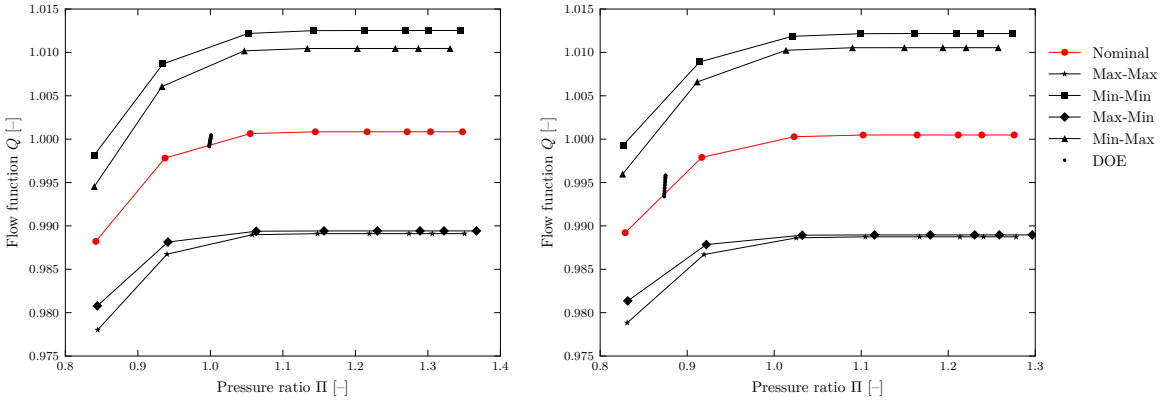

(a) Rotor phase angle variations for ROC (left) and Q4 (right).

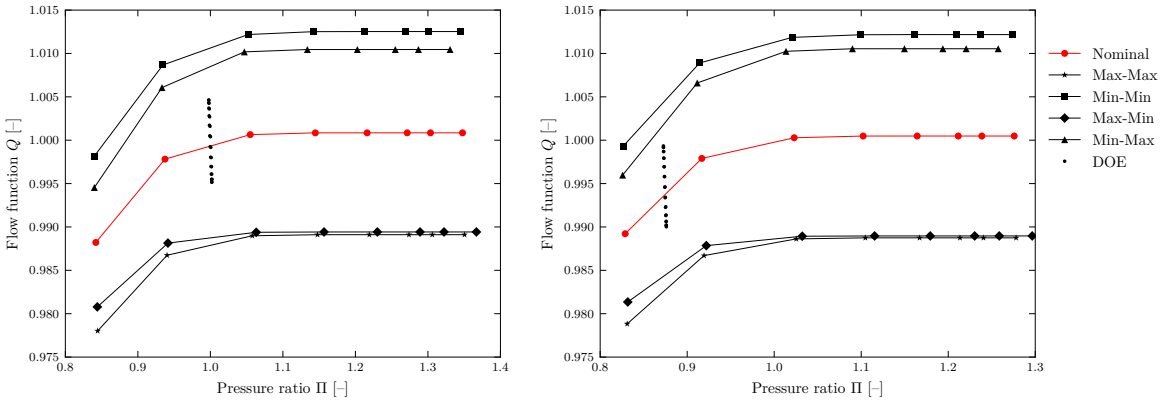

(b) Stator phase angle variations for ROC (left) and Q4 (right).

Figure 4.9: Turbine maps of flow function Q versus pressure ratio Π for the design cases in which only phase angle was varied in the sinusoidal function $f_{\sin}$. The period for both phase angle variations was set to $n_i = 1$. Results are normalised relative to results for nominal blade design and ROC.

Figure 4.10 shows the turbine map of efficiency η versus pressure ratio Π for the two phase angle variation cases where the period was set to unity (n_i). Figure 4.10a show the performance scatter when the rotor phase angle was varied, while Figure 4.10b instead show the scatter when the stator phase angle was varied.

Comparing the scatter in efficiency for the two cases, one finds that difference in scatter between varying the phase angles of the rotor and the stator, respectively, is not as significant as it was for the flow function. The configurations simulated with Q4 operating conditions (right) have an improved performance, relative to nominal design results, while configurations simulated with ROC are more evenly distributed across nominal design results.

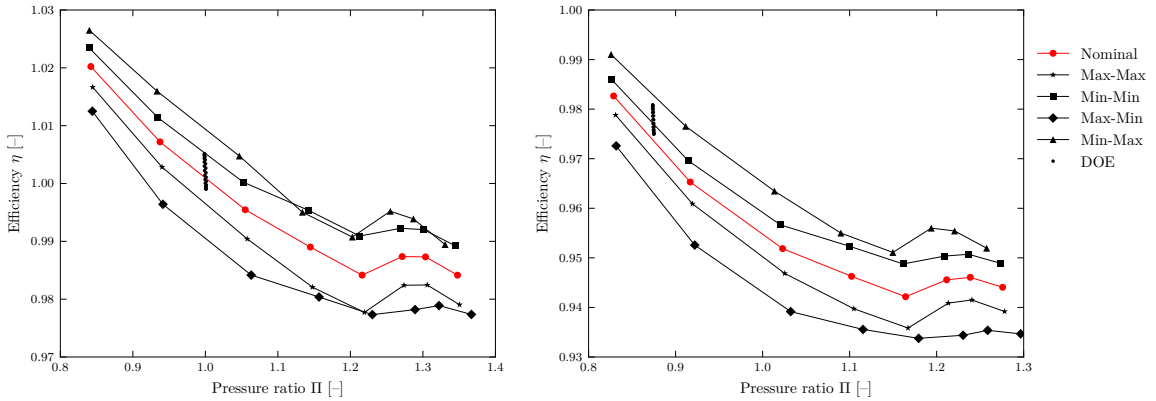

(a) Rotor phase angle variations for ROC (left) and Q4 (right).

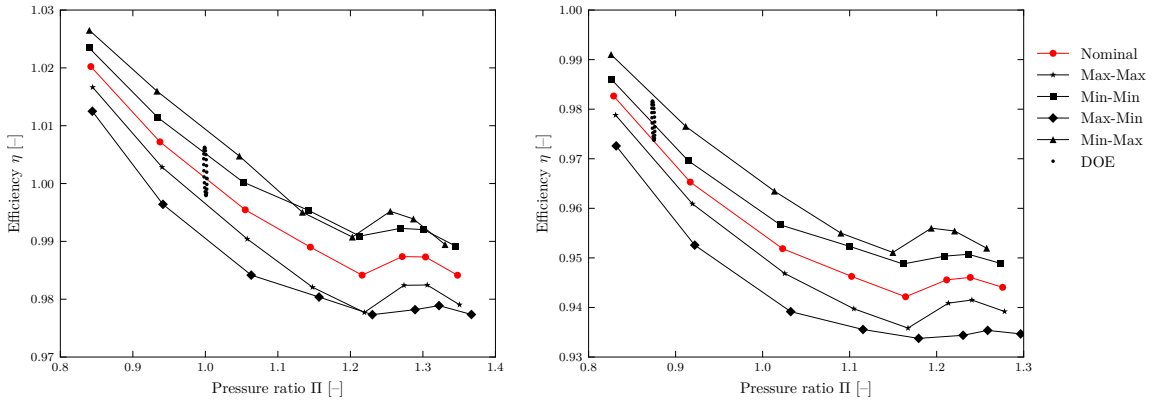

(b) Stator phase angle variations for ROC (left) and Q4 (right).

Figure 4.10: Turbine maps of efficiency η versus pressure ratio Π for the design cases in which only phase angle was varied in the sinusoidal function $f_{\sin}$. The period for both phase angle variations was set to $n_i = 1$. Results are normalised relative to results for nominal blade design and ROC.

Figure 4.11 shows the corresponding rotor profiles that resulted in minimum (4.11a) and maximum (4.11b) efficiency, respectively. Again, it was found that minimum and maximum efficiency was obtained for the same configuration for the two qualification points. Minimum efficiency was obtained for a rotor phase angle of $\varphi_r = 15.0°$, while maximum efficiency was obtained for the rotor phase angle $\varphi_r = 195.0°$ (this corresponds to ID=2 and ID=14 respectively in Table A.3 in Appendix A). Similar to the Latin hypercube design, Figures 4.11a and 4.11b differ in trailing edge thickness, with the profile for maximum efficiency having a sharper trailing edge than the profile for minimum efficiency. They also differ in suction surface curvature downstream throat, i.e. unguided turning.

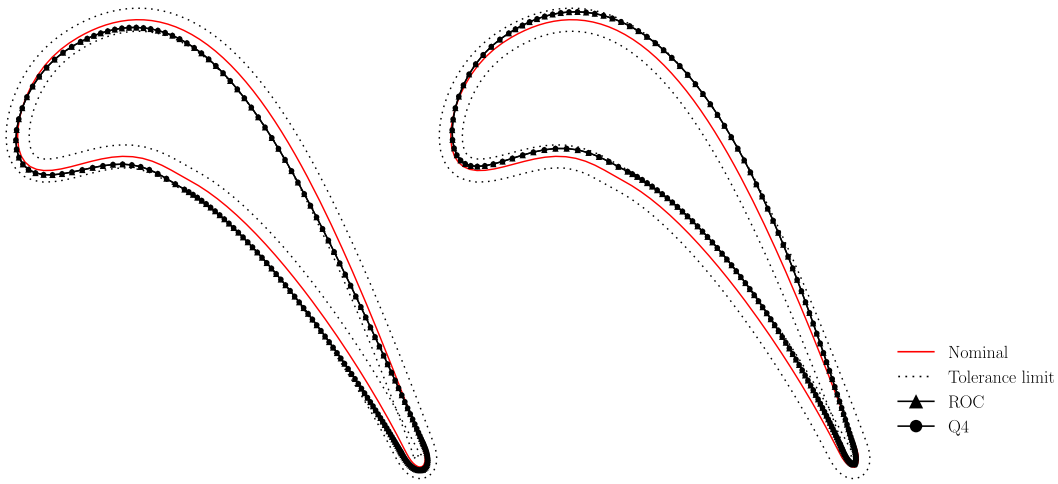

Figure 4.11: Rotor profiles for (a) minimum and (b) maximum efficiency for the rotor phase angle variation case with constant period $n_r = 1$. The profiles for the respective qualification points, ROC and Q4, are identical as minimum and maximum efficiency occurs for the same configurations for both qualification points. The solid (red) line represents nominal design, while the dotted (black) lines outline the profile tolerances. Note that geometry variations have been magnified for better visualisation.

Table 4.2 shows a summary of the rotor phase angle variation case with respect to configurations resulting in maximum and minimum efficiency for the two qualification points. Again, it should be pointed out that the values for flow function listed in Table 4.2 are not the global minimum and maximum values, but rather the values corresponding to minimum and maximum efficiency, respectively. The relationship between efficiency and flow function versus phase angle is shown in Figure 4.12.

Table 4.2: Summary of phase angle variation results showing normalised values of η_{min} and η_{max}, as well as corresponding normalised values of the flow function. Results are normalised against results for nominal blade design simulated with ROC.

Qualification point	η_{min}	η_{max}	Q_{min}	Q_{max}
ROC	0.9990	1.0052	0.9940	0.9996
Q4	0.9749	0.9809	0.9953	1.0020

Figure 4.12 shows efficiency versus phase angle (4.12a) and flow function (4.12b) and clearly shows that maximum efficiency does not correspond to maximum flow function, and vice versa. The same conclusion may be made regarding the minimum values. It should be noted that Figure 4.12 is for ROC. The same trend was seen for Q4 operating conditions and is shown in B.1a in Appendix B.1.

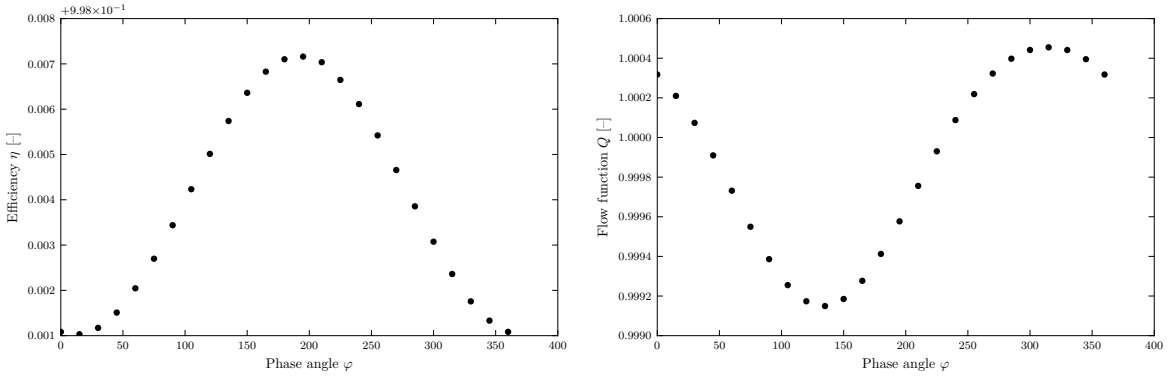

(a) **(b)**

Figure 4.12: Efficiency η (a) and flow function Q (b) versus rotor phase angle variation for ROC when varying only the phase angle in the sinusoidal function $f_{\sin}$. period is constant $n_r = 1$.

Figure 4.13 shows the corresponding stator profiles that resulted in minimum (4.13a) and maximum (4.13b) efficiency, respectively. As opposed to previous results, for this case it was not found that maximum efficiency occurred for the same configuration for both qualification points. For ROC, maximum efficiency was obtained for a stator phase angle $\varphi_s = 255.0°$, whereas for Q4 operating conditions, the phase angle for maximum efficiency was instead $\varphi_s = 240.0°$, however, this difference is not discernible in Figure 4.13. Minimum efficiency, on the other hand, was achieved for the same configuration for both qualification points and occurred at a stator phase angle of $\varphi_s = 75.0°$. These values correspond to ID18, ID17 and ID6, respectively, in Table A.4 in Appendix A.

As can be seen in Figure 4.13, the profile for maximum efficiency has a strong taper from leading to trailing edge, while the profile for minimum efficiency has little to no taper from leading to trailing edge. The trailing edge in 4.13b is also noticeable thinner than the trailing edge in 4.13a. Furthermore, there is a visible difference in the thickness of the leading edge between the two profiles.

Figure 4.13: Stator profiles for (a) minimum and (b) maximum efficiency for the stator phase angle variation case with constant period $n_s = 1$. While maximum efficiency (b) is not achieved for identical phase angle for the two qualification points, the difference in phase angle (15°) is not discernible. The solid (red) line represents nominal design, while the dotted (black) lines outline the profile tolerances. Note that geometry variations have been magnified for better visualisation.

Table 4.3 shows a summary of the rotor phase angle variation case with respect to configurations resulting in maximum and minimum efficiency for the two qualification points.

Table 4.3: Summary of phase angle variation results showing normalised values of η_{min} and η_{max}, as well as corresponding normalised values of the flow function. Results are normalised against results for nominal blade design simulated with ROC.

Qualification point	η_{min}	η_{max}	Q_{min}	Q_{max}
ROC	0.9990	1.0063	0.9970	1.0027
Q4	0.9737	0.9816	0.9923	0.9979

Figure 4.14 shows efficiency versus phase angle (4.14a) and flow function (4.14b) for ROC. The relationship between efficiency and stator phase angle, and flow function and stator phase angle, appears to be inverted to the relationships shown in 4.12. Similar results were seen for Q4 operating conditions and are shown in B.1b in Appendix B.1.

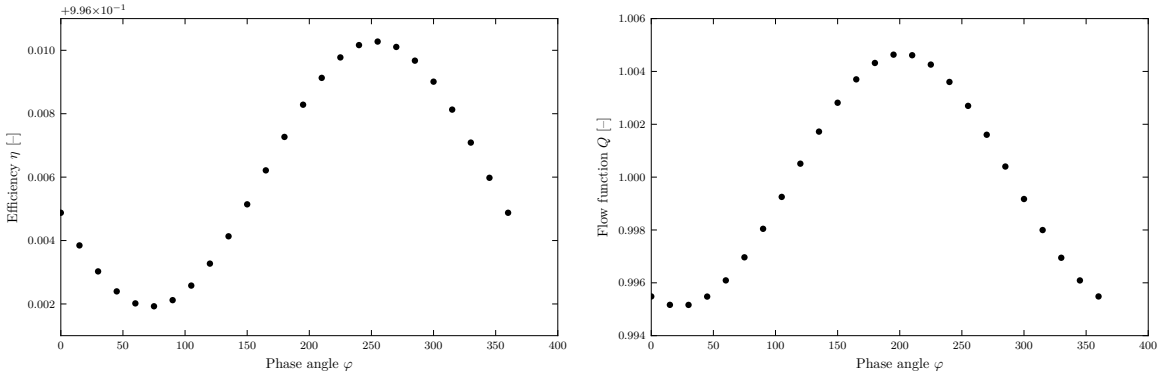

(a) **(b)**

Figure 4.14: Efficiency η (left) and flow function Q (right) versus rotor phase angle variation when varying only the phase angle in the sinusoidal function $f_{\sin}$. Period is constant $n_s = 1$.

4.2.3.2 Dual period

The phase angle variation cases were repeated but with a dual period, $n_i = 2$, for the blade being modified. Similar results were produced for these cases and are shown in Figures B.2 and B.3 in Appendix B.2. As for the case with a single period, varying the stator phase angle seems to have a more significant effect in terms of flow function and efficiency, and a larger variation in terms of efficiency can be observed for the case when $n_i = 2$.

Similar relationships between efficiency and phase angle variation, and flow function and phase angle, were seen, although the peaks of these were somewhat shifted compared to those for the case with a single period. These are shown in Figures B.4 and B.5 for the respective qualification points in Appendix B.2.

When varying the rotor phase angle, it was observed that minimum and maximum efficiency occurred for phase angles of $\varphi_r = 30°$ and $\varphi_r = 210°$, respectively, for both qualification points (ID3 and ID15, respectively, in Table A.5). Figure 4.15 shows the blade profiles for these configurations, while Table 4.4 shows a summary of values for minimum and maximum efficiencies, and corresponding flow function values.

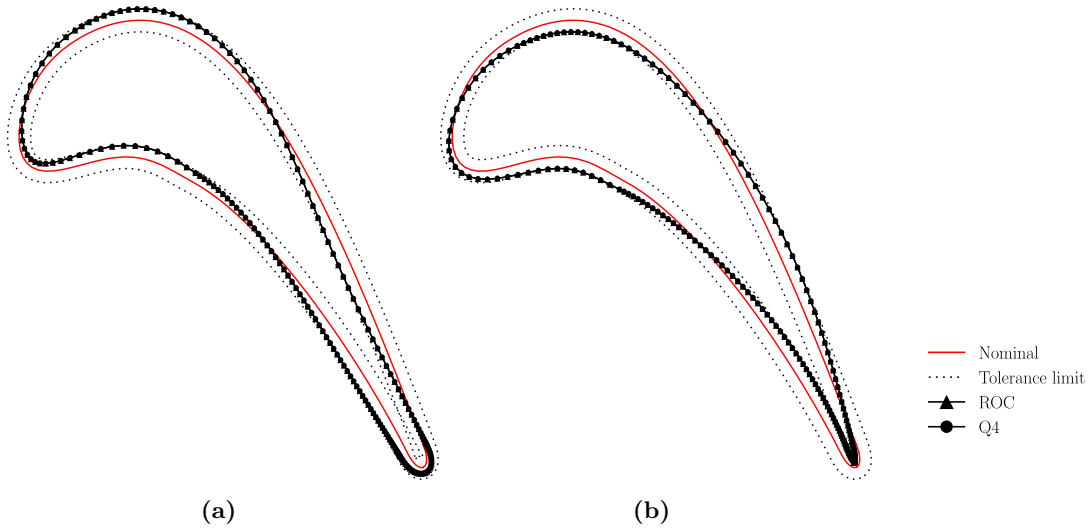

(a) **(b)**

Figure 4.15: Rotor profiles for (a) minimum and (b) maximum efficiency for the rotor phase angle variation case with constant period $n_r = 2$. The solid (red) line represents nominal design, while the dotted (black) lines outline the profile tolerances. Note that geometry variations have been magnified for better visualisation.

Table 4.4: Summary of phase angle variation results showing normalised values of η_{min} and η_{max}, as well as corresponding normalised values of the flow function. Results are normalised against results for nominal blade design simulated with ROC.

Qualification point	η_{min}	η_{max}	Q_{min}	Q_{max}
ROC	0.9985	1.0056	1.0000	0.9997
Q4	0.9746	0.9812	0.9951	0.9942

Varying stator phase angle resulted in minimum and maximum efficiencies for configurations with phase angle $\varphi_s = 120°$ and $\varphi_s = 300°$, respectively (ID9 and ID21, respectively, in Table A.6). Again, minimum and maximum efficiency for the two qualification points coincided for the same configurations, which are visualised in Figure 4.16. Table 4.5 below lists the efficiency results for the stator phase angle variation, as well as the corresponding flow function values.

Figure 4.16: Stator profiles for (a) minimum and (b) maximum efficiency for the stator phase angle variation case with constant period $n_s = 2$. The solid (red) line represents nominal design, and the dotted lines represent profile tolerances. Note that geometry variations have been magnified for better visualisation.

Table 4.5: Summary of phase angle variation results showing normalised values of η_{min} and η_{max}, as well as corresponding normalised values of the flow function. Results are normalised against results for nominal blade design simulated with ROC.

Qualification point	η_{min}	η_{max}	Q_{min}	Q_{max}
ROC	0.9957	1.0078	0.9943	1.0046
Q4	0.9719	0.9823	0.9907	0.9979

4.3 Impact of tolerances

The results presented in Section 4.2 demonstrate the impact of manufacturing tolerances on turbine performance. As can be seen in the results from the profile tolerance design case (Section 4.2.1), varying the blade profile between maximum and minimum profile tolerance values does

not significantly impact performance. The limiting curves for flow function or mass flow are due to the stator-rotor configurations maximum-maximum and minimum-minimum profile tolerance. For efficiency, on the other hand, the limiting curves are due to the stator-rotor configurations minimum-maximum and maximum-minimum profile tolerance.

As mentioned, results have been normalised with respect to nominal blade design evaluated at reference operating conditions, which corresponds to a point located at unity on both the $x-$ and $y-$axis in the turbine maps presented in Section 4.2.1. With respect to this point, it can be seen that the profile tolerances for reference operating conditions result in deviations less than 1.5% for both flow function Q and efficiency η. When considering Q4 operating conditions, deviation appears to be more significant. However, it is important to keep in mind that these results are also normalised with respect to reference operating conditions.

When considering subsequent design cases, such as the LHS design case (Sections 4.2.2) and phase angle variation cases (Section 4.2.3), it was seen that performance for these geometry variations fall between the limiting curves for mass flow and efficiency mentioned in the paragraph above (and Section 4.2.1) i.e. no greater deviation in performance is observed, although this is of course dependent on the tolerances considered. Therefore, it is seen that geometry variations of the blade profile, within the current manufacturing tolerances, does not impact turbine performance markedly, despite this geometry variation being described by a sinusoidal function. The main takeaway from this is that geometric variability of blade profiles has a limited impact on turbine performance, as long as the amplitude of the variability is limited by current manufacturing tolerances. However, it is important to recall that the developed method makes the assumption that all blades within a row have identical geometry variations (see Section 1.2. This will no doubt affect simulations results, however it is difficult to say whether or not this assumption over- or underestimates the observed results

With the current method, it is possible to investigate alternate tolerances which may aid in future decisions and tolerance design. Depending on performance criteria and requirements, the results propose the possibility of employing alternate manufacturing tolerances. Tolerance design is a balance between manufacturing cost and consequential penalties in performance. However, the gap between these two may perhaps be reduced through tolerance designs in which profile tolerance varies depending on position along the blade circumference. The following sections aim at presenting areas which may be more sensitive to tolerance design and performance impact.

4.3.1 Efficiency and trailing edge radii

Based on the profiles shown in Figures 4.11 and 4.13, and the recommendations presented in Section 2.4.4.1, it was hypothesised that the trailing edge radius was one of the more significant parameters of the blade profile in terms of performance, as it was seen that efficiency seemed to decrease with an increase trailing edge radius. It should be noted that, when referring to trailing edge *radius*, it is really the *thickness* of the trailing edge that is considered (see Figure 2.5).

In order to validate this proposed correlation, the efficiency was plotted against trailing edge radius for the respective configurations in the phase angle variation cases. The trailing edge radius R_{TE} was calculated by calculating the distance between points LS1 and US0 (see Figure 3.2) according to

$$R_{TE} = \sqrt{(x_{LS1} - x_{US0})^2 + (r\theta_{LS1} - r\theta_{US0})^2} \tag{4.1}$$

where the $r\theta-$coordinates for the respective points were calculated according to Eq (3.2). To give the reader an idea of the position of US0 and LS1 relative to the trailing edge, the distance from the TE to US0 and LS1, respectively, make up less than 2% of the circumference s_N of the blade (as defined in Section 3.2.1). The trailing radius was calculated for the section in the point

set corresponding to the blade mid span, however, this value should not deviate excessively if calculated for another section.

Figure 4.17 shows the efficiency versus trailing edge radius; 4.17a corresponds to the cases for single period ($n_i = 1$) while 4.17b corresponds to the cases for dual period ($n_i = 2$). Each of the figures presented contains two ellipses, one for each of the qualification points, ROC and Q4, respectively. The slopes in Figures 4.17a and 4.17b show that there is a correlation between efficiency and trailing edge radii where efficiency decreases with increasing trailing edge radius; this is especially visible in the figures for when the stator phase angle was varied (Figure 4.17a right and 4.17b right). The cases with dual period (4.17b) result in a steeper slope.

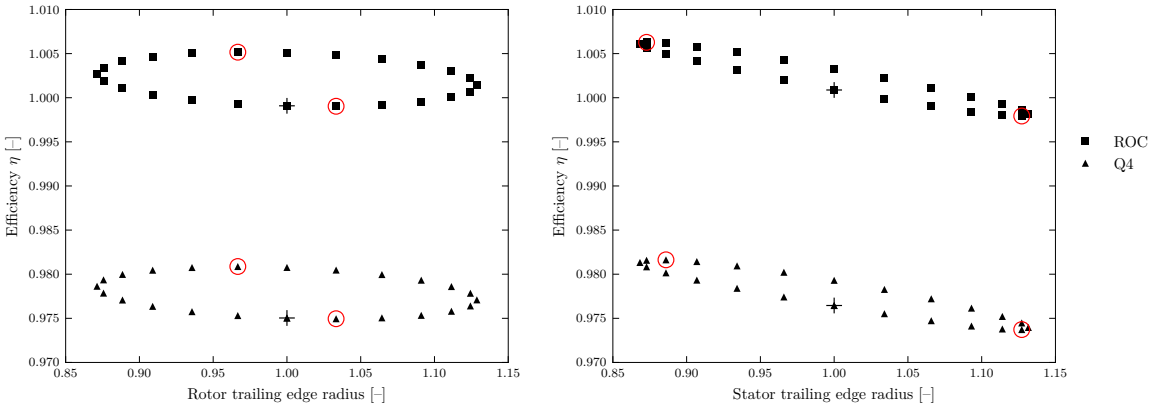

(a) Single period $n_i = 1$

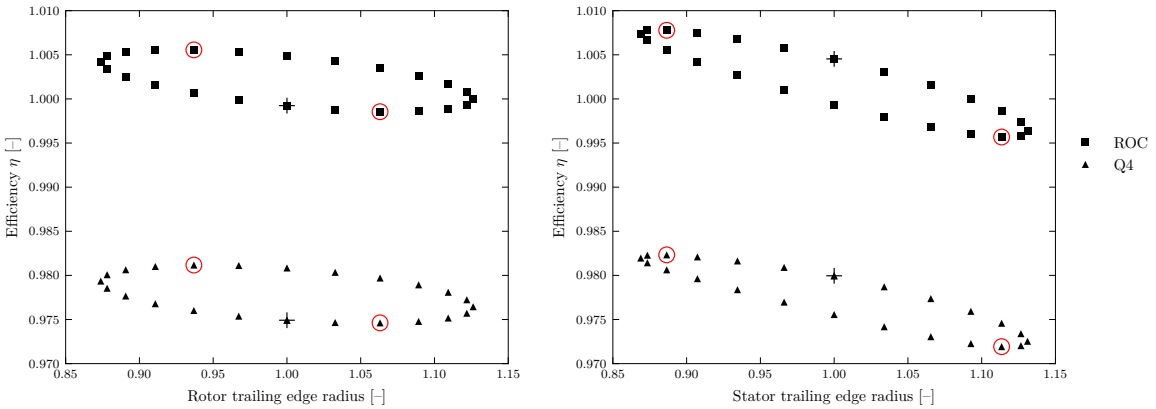

(b) Dual period $n_i = 2$

Figure 4.17: Efficiency η versus rotor trailing edge radius (left) and stator trailing edge radius (right) for the two phase angle variation cases. Points circumscribed with a solid (red) line represent configurations for minimum and maximum efficiency, and points indicated with a plus (+) represent configurations with $\varphi_i = 0 = 360°$. Trailing edge radii are calculated according to Eq (4.1) and are normalised against the nominal trailing edge radius, and efficiencies are normalised against results for nominal blade design simulated with ROC.

Furthermore, it seems as though each trailing edge radius results in two different efficiencies, however, it should be taken in to account that there is in fact an ever so slight deviation in trailing edge radius for two points that appear vertically aligned. The points indicated with a plus + symbol, corresponding to a (normalised) trailing edge radius equal to unity, are the configurations for which the phase angles $\varphi = 0 = 360°$ – for these angles, f_{sin} vanishes and the trailing edge radius is equal to the nominal trailing edge radius. As can be seen, this occurs for the lower of the points where $r_{TE} = 1$ (except for the the stator phase angle variation case for dual period, Figure 4.17b right). From this point, the points proceed in a counter-clockwise direction for increasing phase angle φ. The other point in which trailing edge radius equals

unity corresponds to $\varphi = 180°$, for which $f_{\sin}$ again vanishes. This counter-clockwise manner is concurrent for all of the cases, except for the the stator phase angle variation case for dual period (Figure 4.17b right). For this case, the points instead proceed in a clockwise direction.

While there appears to be some correlation between efficiency and trailing edge radii, it should be recognised that the minimum and maximum efficiencies for the respective cases – the points circumscribed with a solid (red) line in Figure 4.17 – do not correspond to the profiles with the greatest and smallest trailing edge radii. This may be seen in Tables 4.6 and 4.7 which shows the efficiencies corresponding to the trailing edge radii extremes; comparing the values in Table 4.6 and 4.7 with corresponding value in Tables 4.2–4.5, it becomes apparent that the values differ.

Table 4.6: Efficiencies for minimum and maximum TE radii for rotor phase angle variation cases.

	TE radius	η_{ROC}	η_{Q4}
$n_r = 1$	0.8713	1.0027	0.9786
	1.1287	1.0014	0.9771
$n_r = 2$	0.8738	1.0042	0.9793
	1.1262	1.0000	0.9764

Table 4.7: Efficiencies for minimum and maximum TE radii for stator phase angle variation cases.

	TE radius	η_{ROC}	η_{Q4}
$n_s = 1$	0.8684	1.0061	0.9813
	1.1316	0.9981	0.9740
$n_s = 2$	0.8689	1.0074	0.9819
	1.1311	0.9964	0.9725

Finally, when comparing the results for single period with those for dual period, another fact becomes apparent. Efficiency corresponding to minimum trailing edge radius increases between $n_i = 1$ and $n_i = 2$ – even though the minimum trailing edge radius also increases. Similarly, efficiency corresponding to maximum trailing edge radius decreases between $n_i = 1$ and $n_i = 2$ – even though the maximum trailing edge radius also decreases. This is applicable to both the stator and rotor, and both qualification points ROC and Q4, as may be seen in Tables 4.6 and 4.7, respectively.

Although this does not necessarily invalidate the correlation between trailing edge radii and efficiency, it does suggest that efficiency is not solely dependent on trailing edge radius, but in fact that there are other parameters that need to be considered and analysed. It may prove advantageous with a stricter tolerance design near the blades' trailing edges, and may also mitigate efforts needed to characterise these unknown parameters by reducing the impact of trailing edge losses in future blade designs.

4.3.2 Unguided tuning

While unguided turning has not been quantitatively assessed in this project, the potential effects may be qualitatively reviewed. This is done in particular with respect to the rotor profiles resulting in minimum and maximum efficiencies presented in previous sections. Consistent for all of the design cases is that rotor profiles resulting in minimum efficiency appear to be more less curved and with more straight-backed suction surfaces, which is often the case in supersonic turbines with limited unguided turning [10].

Conversely, rotor profiles for maximum efficiency have a much more prominent curvature, both when considering the suction and pressure side. These more pronounced curvatures are predicted to provide a longer flow path as well as an increased amount of unguided turning downstream of the throat. Consequently, it may be beneficial with a tolerance design aimed at guaranteeing a unguided turning angle within recommended values (as mentioned in Section 2.4.4.2) in order to avoid performance penalties.

5

Conclusion

In this project, a rational method to vary blade profile variations in axial flow turbomachines has been developed. The method has been utilised to study the impact of simulated manufacturing tolerances on turbine performance. The method allows blade profiles for both stator and rotor blades to be modified with a sinusoidal function, of which amplitude A_i, period n_i, and phase angle φ_i, may be varied. The method has been implemented and evaluated through CFD simulations in order to investigate the impact of geometry variations within current manufacturing tolerances on turbine performance for a liquid hydrogen turbine. The impact on performance was quantified mainly with respect to efficiency η and flow function Q.

It was observed that geometry variations of blade profiles within current manufacturing tolerances have a limited impact on turbine performance as the variations are within the tolerance band. However, the consequences of a seemingly limited impact can be debated, as a a seemingly small reduction in e.g. efficiency may still be considered significant as it may result in a reduction of payload.

The method is an adequate initial approach at investigating performance impact for geometry variations within manufacturing tolerances. The method provides a reasonable estimation of the effects of current manufacturing tolerances on turbine performance, and may be implemented in future tolerance designs. However, it should be noted that the current method has been implemented for a simplified model, which may affect the results. Although the geometry of the turbine has been simplified by neglecting for example the clearance gap, the results may still be valid as such. However, if variations in clearance gap are considered simultaneously with the profile variations covered in this thesis, it may be observed that clearance gap variations have a much larger impact on the turbine characteristics.

In order to get a better understanding and perhaps increase the validity of the results, suggestions for future work include implementing the method on more complex models. This includes consideration to clearance gaps, which have been omitted in this project, as well as investigating effects for when geometry variations are not identical for all blades in a given row. Regarding the method development, it is recommended to investigate alternate profile variations, as well as performance impacts for profiles with varying tolerance design along the blade profile. Finally, investigating the feasibility of fusing the developed method (2LOOP) with GKN Aerospace's blade optimisation method (theLOOP) with the possibility of combining blade design and tolerance design optimisation would be of value.

Bibliography

[1] "GKN Aerospace wins major contracts from Airbus Safran Launchers for Ariane 6 rocket engine sub-systems," Available at http://www.gkn.com/media/News/Pages/GKN-Aerospace-wins-major-contracts-from-Airbus-Safran-Launchers-for-Ariane-6-rocket-engine-sub-systems.aspx, May 2016, [Online; posted 24-May-2016].

[2] S. Dixon and C. Hall, *Fluid mechanics and Thermodynamics of Turbomachinery*, 7th ed. Elsevier, 1995.

[3] Duk, "Staged combustion rocket cycle," Available at https://commons.wikimedia.org/wiki/File:Staged_combustion_rocket_cycle.svg, Oct. 2008, licensed under CC BY-SA 3.0 (https://creativecommons.org/licenses/by-sa/3.0/deed.en), modified from original. [Online; accessed 24-May-2016].

[4] ——, "Gas generator rocket cycle," Available at https://commons.wikimedia.org/wiki/File:Gas_generator_rocket_cycle.svg, Oct. 2008, licensed under CC BY-SA 3.0 (https://creativecommons.org/licenses/by-sa/3.0/deed.en), modified from original. [Online; accessed 24-May-2016].

[5] ——, "Expander rocket cycle," Available at https://commons.wikimedia.org/wiki/File:Expander_rocket_cycle.svg, Oct. 2008, licensed under CC BY-SA 3.0 (https://creativecommons.org/licenses/by-sa/3.0/deed.en), modified from original. [Online; accessed 24-May-2016].

[6] M. Olausson, "Design Practice for LPC Blade Aero Design Based on Design of Experiments," GKN Aerospace, SE-461 81 Trollhättan, Sweden, Tech. Rep. VOLS:10172608, September 2016.

[7] M. D. McKay, R. J. Beckman, and W. J. Conover, "Comparison of Three Methods for Selecting Values of Input Variables in the Analysis of Output from a Computer Code," *Technometrics*, vol. 21, no. 2, pp. 239–245, 1979.

[8] B. Andersson, R. Andersson, L. Håkansson, M. Mortensen, R. Sudiyo, and B. van Wachem, *Computational Fluid Dynamics for Engineers*. Cambridge University Press, 2011.

[9] J. Andersson and I. Ljungkrona, "Performance assessment of subsonic turbines, based on engine tests," GKN Aerospace, SE-461 81 Trollhättan, Sweden, Tech. Rep. VOLS:10187877, September 2014.

[10] "Liquid Rocket Engine Turbines, Nasa Space Vehicle Design Criteria (Chemical)," National Aeronautics and Space Administration (NASA), Tech. Rep. SP-8110, January 1974.

[11] M. Olausson, "PollyGraph - A Blade Design Tool," GKN Aerospace, Tech. Rep. VOLS:10186012, September 2014.

[12] L. Ljungkrona, "Point set data format for stacked blade sections," GKN Aerospace, SE-461 81 Trollhättan, Sweden, Tech. Rep., November 2012.

[13] A. D. Lee, "pyDOE: Design of experiments for Python," Available at http://pythonhosted.org/pyDOE/.

[14] H. K. Versteeg and W. Malaskekera, *An Introduction to Computational Fluid Dynamics: The Finite Volume Method*, 2nd ed. Pearson Education Limited, 2007.

[15] M. Billson, "Meshing using meshblade and g3dmesh," GKN Aerospace, SE-461 81 Trollhättan, Sweden, Tech. Rep. VOLS:10098094, November 2010.

[16] N. Andersson, *G3D::Flow – A Massively Parallel CFD Solver Framework*, Department of Applied Mechanics, Division of Fluid Mechanics, Chalmers University of Technology.

[17] ——, *VolSol++ – A Common Massively Parallel Platform for In-house CFD/CAA/FSI @ VAC*, GKN Aerospace, SE-461 81 Trollhättan, Sweden, Oct. 2009.

A

Design tables

Table A.1: Design table for profile tolerance case. "Maximum" and "minimum" amplitude refer to the maximum and minimum allowable values with respect to the profile tolerances. For confidentiality reasons, these values are withheld.

ID	A_s	n_s	φ_s	A_r	n_r	φ_r
1	Nominal	0	90	Nominal	0	90
2	Maximum	0	90	Maximum	0	90
3	Minimum	0	90	Minimum	0	90
4	Maximum	0	90	Minimum	0	90
5	Minimum	0	90	Maximum	0	90

Table A.2: Design table for latin-hypercube design case.

ID	n_s	φ_s	n_r	φ_r	ID	n_s	φ_s	n_r	φ_r	ID	n_s	φ_s	n_r	φ_r
1	8	321	1	196	34	8	289	1	233	68	6	338	3	258
2	6	242	5	74	35	5	69	10	3	69	8	332	4	238
3	10	147	3	97	36	9	47	2	201	70	1	22	8	119
4	10	40	7	60	37	8	126	7	315	71	6	220	8	90
5	6	122	2	97	38	7	112	8	12	72	9	218	10	21
6	5	102	5	109	39	2	299	4	29	73	3	182	4	187
7	9	173	6	203	40	5	208	7	241	74	6	72	4	161
8	4	304	3	313	41	4	293	4	297	75	2	54	6	242
9	4	319	3	157	42	2	352	9	103	76	3	259	2	256
10	2	21	8	112	43	7	57	6	15	77	4	142	7	50
11	3	253	9	295	44	6	277	5	148	78	1	241	10	340
12	2	177	6	181	45	4	223	7	261	79	10	96	3	42
13	7	211	7	107	46	7	353	7	292	80	3	67	7	304
14	7	286	10	35	47	1	18	6	143	81	5	339	9	353
15	2	161	9	226	48	10	270	2	29	82	5	229	10	154
16	7	79	2	63	49	4	163	7	130	83	4	108	8	10
17	4	359	5	322	50	1	203	4	334	84	8	279	8	213
18	8	234	5	189	51	1	30	5	78	85	10	10	8	230
19	3	134	4	174	52	9	345	6	88	86	2	235	4	193
20	8	132	3	126	53	4	214	7	351	87	5	171	8	169
21	8	306	1	82	54	8	298	7	325	88	4	347	4	66
22	9	59	3	51	55	3	264	1	267	89	9	252	8	22
23	6	311	6	306	56	3	151	2	169	90	3	257	8	57
24	2	2	6	178	57	6	193	6	86	91	5	100	4	246
25	4	137	2	331	58	9	34	9	265	92	5	248	9	70
26	7	46	2	208	59	7	314	1	345	93	6	93	8	302
27	8	111	10	270	60	7	83	5	288	94	6	41	9	123
28	5	269	9	282	61	5	5	9	116	95	5	324	5	336
29	3	127	2	216	62	9	29	9	357	96	7	88	3	277
30	8	282	2	346	63	7	11	6	162	97	4	86	5	210
31	1	200	7	279	64	2	331	5	318	98	6	195	4	221
32	9	116	6	134	65	3	169	5	137	99	10	185	3	145
33	2	149	2	249	66	2	62	4	36	100	8	155	3	7
					67	9	189	3	45					

Table A.3: Design table for rotor phase angle variation case and single period $n_r = 1$ (nominal stator design)

ID	n_s	φ_s	n_r	φ_r
1	0	90	1	0
2	0	90	1	15
3	0	90	1	30
4	0	90	1	45
5	0	90	1	60
6	0	90	1	75
7	0	90	1	90
8	0	90	1	105
9	0	90	1	120
10	0	90	1	135
11	0	90	1	150
12	0	90	1	165
13	0	90	1	180
14	0	90	1	195
15	0	90	1	210
16	0	90	1	225
17	0	90	1	240
18	0	90	1	255
19	0	90	1	270
20	0	90	1	285
21	0	90	1	300
22	0	90	1	315
23	0	90	1	330
24	0	90	1	345
25	0	90	1	360

Table A.4: Design table for stator phase angle variation case with single period $n_s = 1$ (nominal rotor design)

ID	n_s	φ_s	n_r	φ_r
1	1	0	0	90
2	1	15	0	90
3	1	30	0	90
4	1	45	0	90
5	1	60	0	90
6	1	75	0	90
7	1	90	0	90
8	1	105	0	90
9	1	120	0	90
10	1	135	0	90
11	1	150	0	90
12	1	165	0	90
13	1	180	0	90
14	1	195	0	90
15	1	210	0	90
16	1	225	0	90
17	1	240	0	90
18	1	255	0	90
19	1	270	0	90
20	1	285	0	90
21	1	300	0	90
22	1	315	0	90
23	1	330	0	90
24	1	345	0	90
25	1	360	0	90

Table A.5: Design table for rotor phase angle variation case and dual period $n_r = 2$ (nominal stator design)

ID	n_s	φ_s	n_r	φ_r
1	0	90	2	0
2	0	90	2	15
3	0	90	2	30
4	0	90	2	45
5	0	90	2	60
6	0	90	2	75
7	0	90	2	90
8	0	90	2	105
9	0	90	2	120
10	0	90	2	135
11	0	90	2	150
12	0	90	2	165
13	0	90	2	180
14	0	90	2	195
15	0	90	2	210
16	0	90	2	225
17	0	90	2	240
18	0	90	2	255
19	0	90	2	270
20	0	90	2	285
21	0	90	2	300
22	0	90	2	315
23	0	90	2	330
24	0	90	2	345
25	0	90	2	360

Table A.6: Design table for stator phase angle variation case and dual period $n_s = 2$ (nominal rotor design)

ID	n_s	φ_s	n_r	φ_r
1	2	0	0	90
2	2	15	0	90
3	2	30	0	90
4	2	45	0	90
5	2	60	0	90
6	2	75	0	90
7	2	90	0	90
8	2	105	0	90
9	2	120	0	90
10	2	135	0	90
11	2	150	0	90
12	2	165	0	90
13	2	180	0	90
14	2	195	0	90
15	2	210	0	90
16	2	225	0	90
17	2	240	0	90
18	2	255	0	90
19	2	270	0	90
20	2	285	0	90
21	2	300	0	90
22	2	315	0	90
23	2	330	0	90
24	2	345	0	90
25	2	360	0	90

B

Results

B.1 Phase angle variation - single period

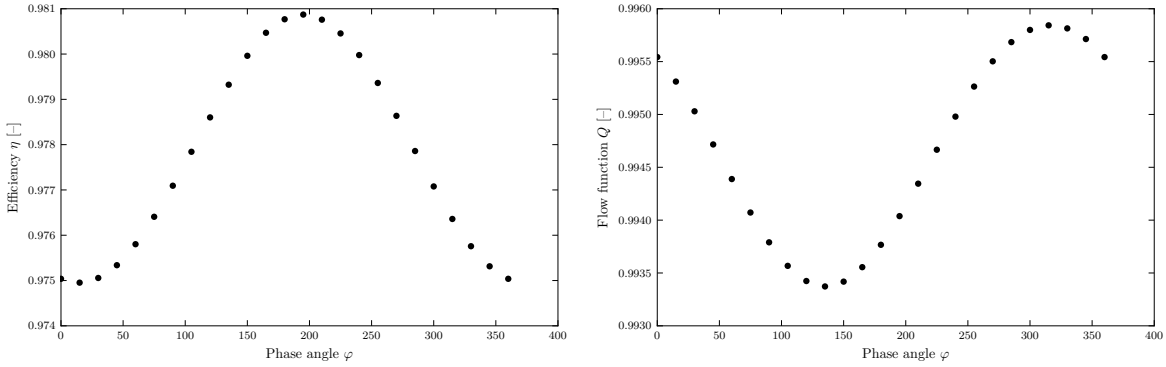

(a) Efficiency η (left) and flow function Q (right) versus rotor phase angle variation

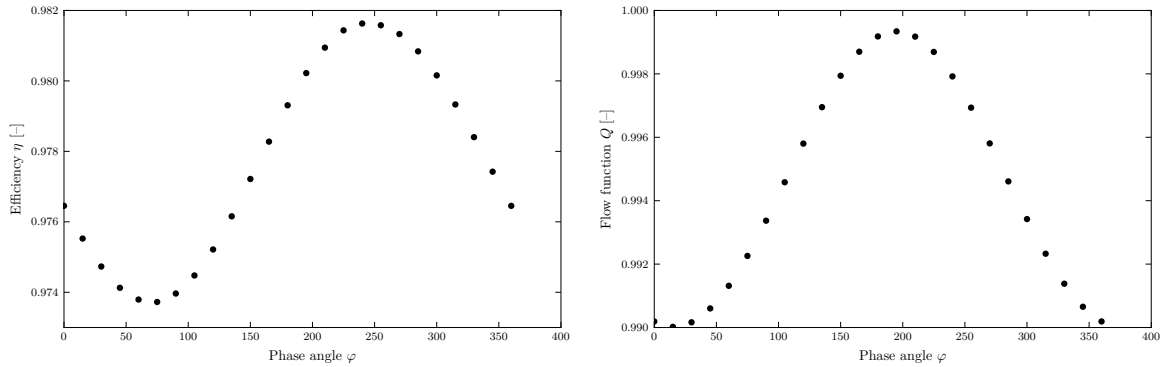

(b) Efficiency η (left) and flow function Q (right) versus stator phase angle variation

Figure B.1: Efficiency η (left) and flow function Q (right) versus (a) rotor phase angle variation and (b) stator phase angle variation for Q4 operating conditions when varying only the phase angle in the sinusoidal function $f_{\sin}$. Periodicity is constant $n_i = 1$. Results are normalised relative to results for nominal blade design and ROC.

B.2 Phase angle - dual period

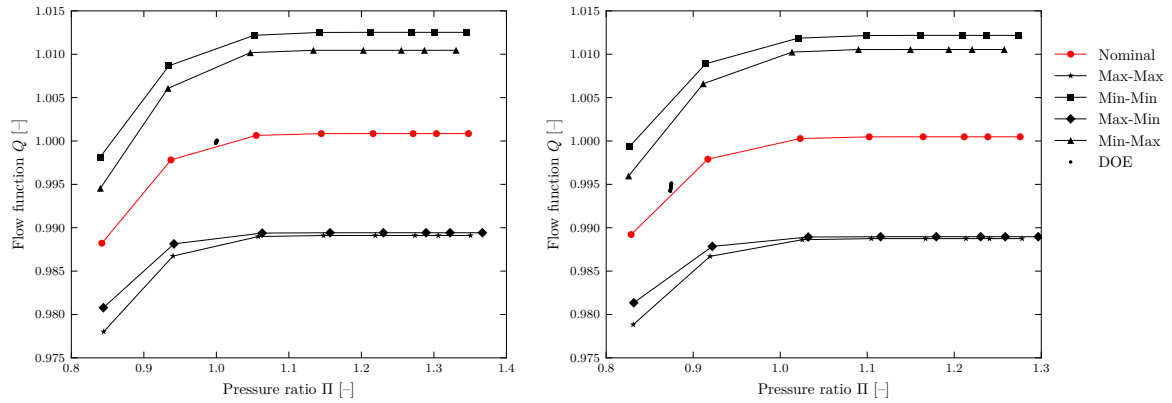

(a) Rotor phase angle variations with ROC (left) and Q4 (right).

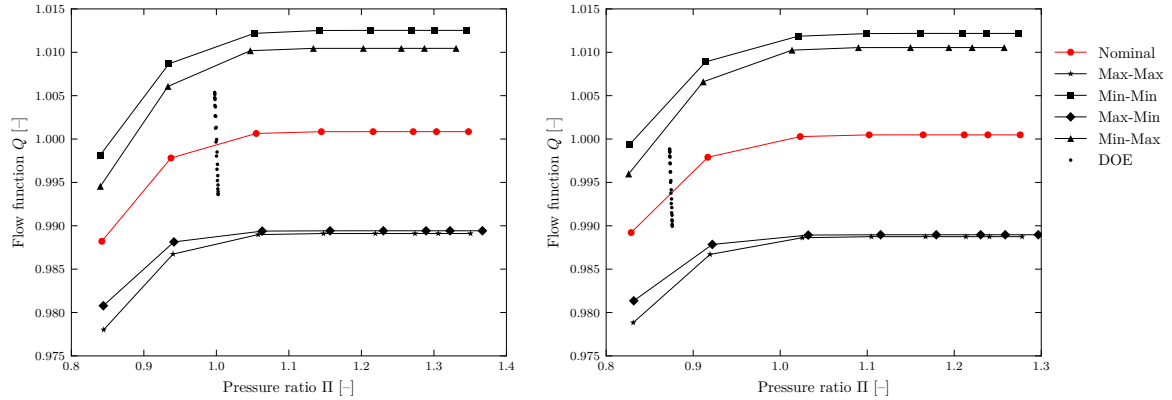

(b) Stator phase angle variations with ROC (left) and Q4 (right).

Figure B.2: Turbine maps of flow function Q versus pressure ratio Π for the design cases in which only phase angle was varied in the sinusoidal function $f_{\sin}$. The periodicity for both phase angle variations was set to $n_i = 2$. Results are normalised relative to results for nominal blade design and ROC.

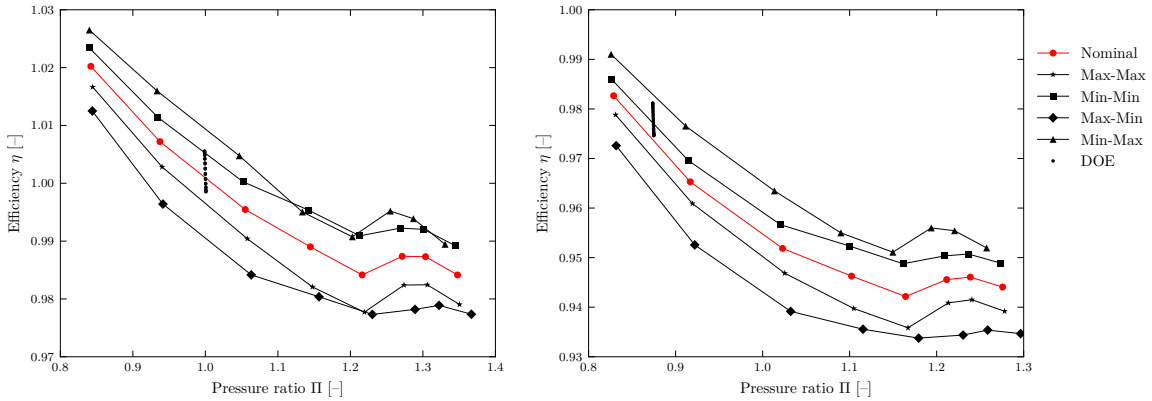

(a) Rotor phase angle variations with ROC (left) and Q4 (right).

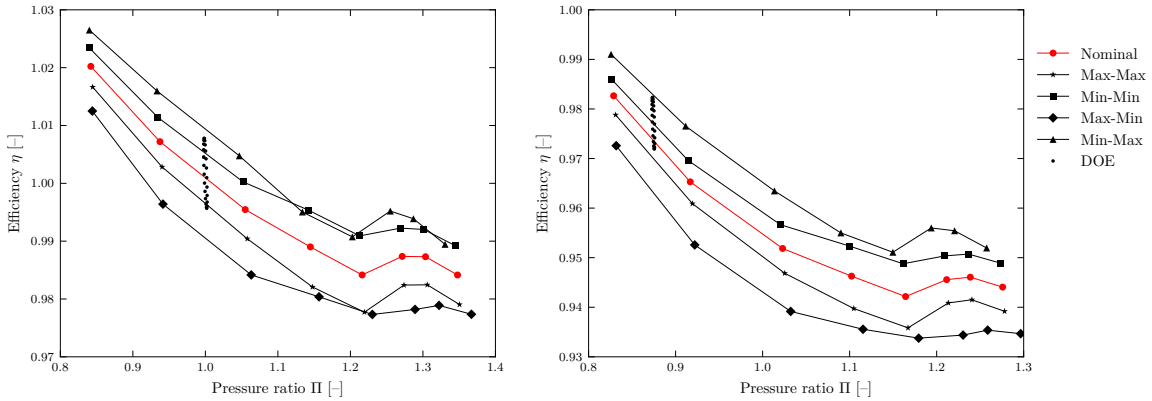

(b) Stator phase angle variations with ROC (left) and Q4 (right).

Figure B.3: Turbine maps of efficiency η versus pressure ratio Π for the design cases in which only phase angle was varied in the sinusoidal function $f_{\sin}$. The periodicity for both phase angle variations was set to $n_i = 2$. Results are normalised relative to results for nominal blade design and ROC.

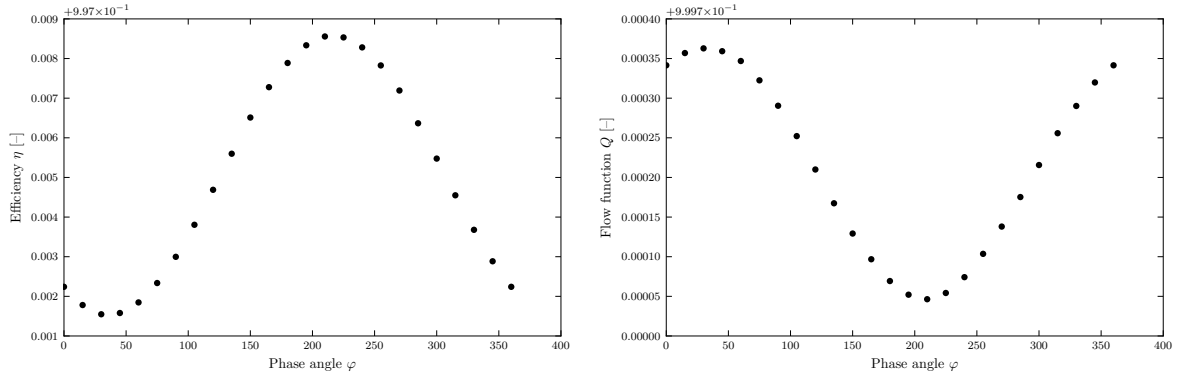

(a) Efficiency η (left) and flow function Q (right) versus rotor phase angle variation

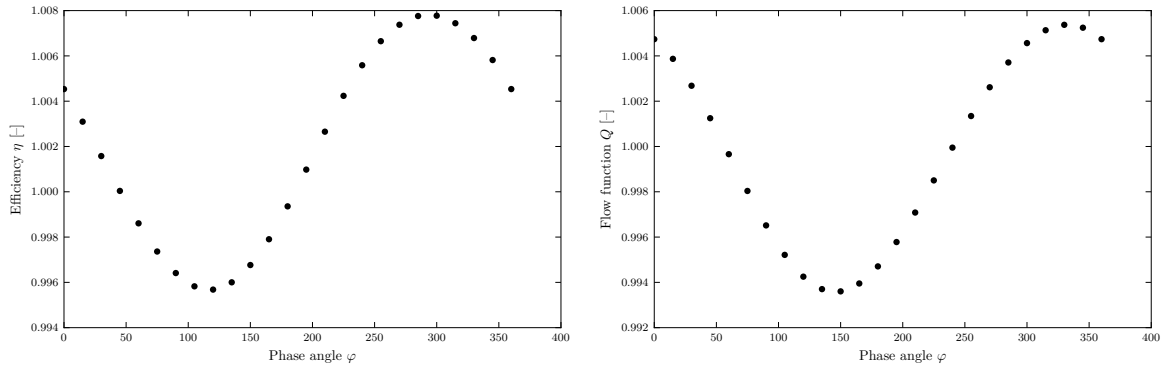

(b) Efficiency η (left) and flow function Q (right) versus stator phase angle variation

Figure B.4: Efficiency η (left) and flow function Q (right) versus (a) rotor phase angle variation and (b) stator phase angle variation and ROC when varying only the phase angle in the sinusoidal function $f_{\sin}$. Periodicity is constant $n_i = 2$. Results are normalised relative to results for nominal blade design and ROC.

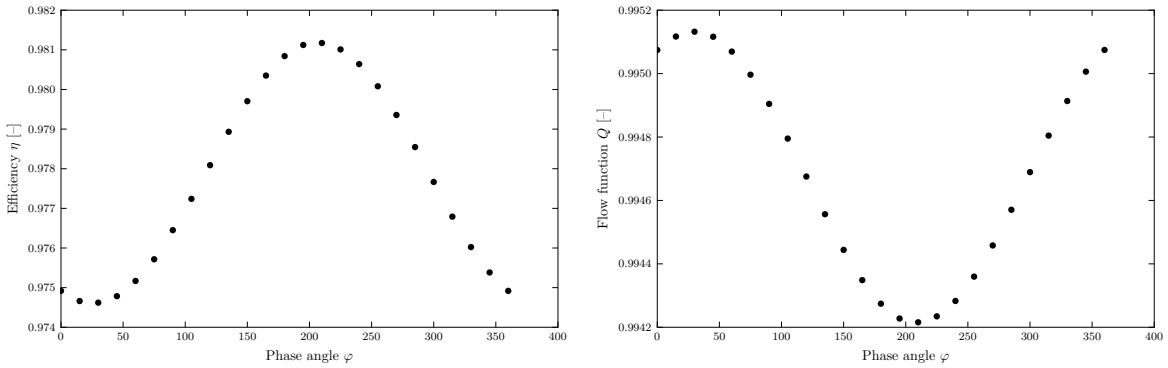

(a) Efficiency η (left) and flow function Q (right) versus rotor phase angle variation

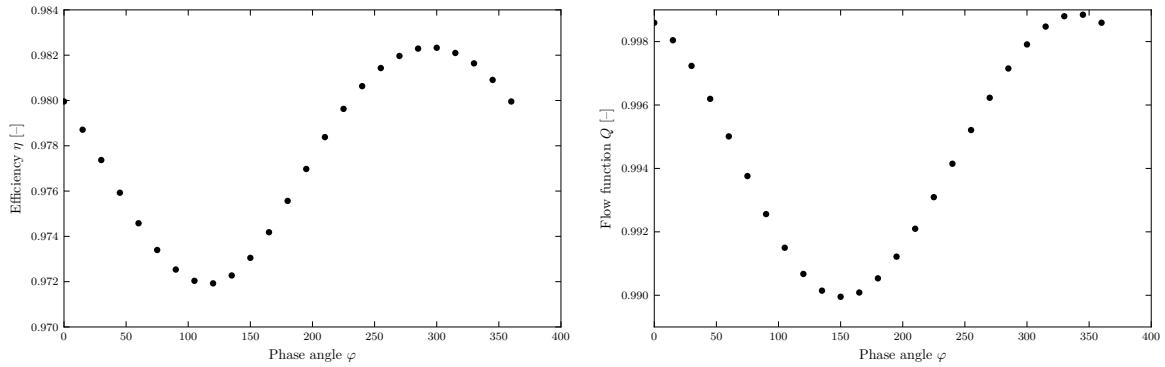

(b) Efficiency η (left) and flow function Q (right) versus stator phase angle variation

Figure B.5: Efficiency η (left) and flow function Q (right) versus (a) rotor phase angle variation and (b) stator phase angle variation and ROC when varying only the phase angle in the sinusoidal function $f_{\sin}$. Periodicity is constant $n_i = 2$. Results are normalised relative to results for nominal blade design and ROC.